**Politecnico di Milano**

SCHOOL OF INDUSTRIAL AND INFORMATION ENGINEERING

Master of Science Degree in Aeronautical Engineering

POLITECNICO
MILANO 1863

# Certification and specific excess power performance tests for a new ultralight aircraft

Candidate:

**Marco Sesso**

**854454**

Supervisor:

**Prof. Lorenzo Trainelli**

Assistant Supervisors:

**Prof. Alberto Rolando**

**Ing. Simone Quaglietta**

**Academic year**

**2017-2018**

*“Quando camminerete sulla terra dopo aver volato,*
*guarderete il cielo perchè là siete stati*
*e là vorrete tornare.”*

Leonardo da Vinci

# Ringraziamenti

Il primo ringraziamento è per il mio relatore Prof. Lorenzo Trainelli senza il quale questa tesi non sarebbe stata possibile. Ringrazio anche il Prof. Alberto Rolando per il supporto, l'Ing. Nando Groppo per la disponibilità e la cordialità dimostrata nelle giornate passate a Mezzana Bigli.

Un sentito grazie all'amico Simone Quaglietta, ottimo pilota con cui ho passato le molte ore a bordo del velivolo e nell'hangar e che è sempre stato fonte di preziosi ed utili suggerimenti a qualsiasi ora ed in qualsiasi giorno.

Un grazie particolare va alla mia famiglia, a mia mamma e mio papà, a mia sorella Giulia ed alla mia fidanzata Arianna per avermi supportato, sopportato e spronato ad andare avanti durante questi anni di studio. Ringrazio anche i miei nonni e ricordo mio nonno, che sarà sicuramente contento del risultato raggiunto.

Infine, un sincero ringraziamento va ai miei amici di università e non, con i quali ho passato innumerevoli ore fuori e dentro le aule a ridere, chiacchierare e anche studiare.

# Abstract

Thanks to the flight testing activity the airworthiness regulations satisfaction of an aircraft can be demonstrated. Moreover, this activity play a key role in the development phase of a new aircraft since it permits to verify if the predictions made in the design phase were correct or not.

This thesis work deals with the certification of a new ultralight aircraft: the TRAIL SBS G70. This is the third prototype and features some improvements derived from the previous test campaigns. The test campaign presented in this work describes the tests performed to complete the certification phase of the aircraft and namely anemometer calibration, stall speed determination and stall behavior.

The results show that the new aircraft satisfies all the requirements imposed by the LTF-UL regulation and so it can be certified.

Finally, a new type of test – Acceleration - Deceleration test – has been performed at the end of the test campaign in order to gather data about the performances of the aircraft. These results have been compared with the ones obtained with a well-known test: the Sawtooth climb test.

# Contents

# List of Figures

# List of Tables

# List of Symbols

| | | |
|---|---|---|
| c | Wing chord | [m] |
| e | Oswald's factor | [-] |
| g | Acceleration of gravity | $[m/s^2]$ |
| h | Altitude | [m] |
| l | Aircraft length | [m] |
| n | Load factor | [-] |
| p | Pitch rate | [deg/s] |
| q | Roll rate | [deg/s] |
| r | Yaw rate | [deg/s] |
| $C_D$ | Drag coefficient | [-] |
| $C_L$ | Lift coefficient | [-] |
| $C_M$ | Complete A/C moment coefficient | [-] |
| $P_b$ | Brake horsepower | [W] |
| $S$ | Wing surface | $[m^2]$ |
| $V_{BG}$ | Best glide speed (maximum endurance) | [km/h] |
| $V_{FC}$ | Fastest climb speed | [km/h] |
| $V_{FE}$ | Maximum speed with flaps extended | [km/h] |
| $V_{GS_{LO}}$ | Ground speed at lift-off | [km/h] |
| $V_{GS_{TD}}$ | Ground speed at touch-down | [km/h] |
| $V_{LO}$ | Lift-off speed | [km/h] |
| $V_{LO_W}$ | Weight reduced lift-off speed | [km/h] |
| $V_{NE}$ | Never exceed speed | [km/h] |
| $V_{NO}$ | Never exceed speed with turbolence | [km/h] |
| $V_R$ | Rotation speed | [km/h] |
| $V_{S1}$ | Stall speed | [km/h] |
| $V_{S0}$ | Stall speed in LND configuration | [km/h] |
| $V_{S1}$ | Stall speed in one specific configuration | [km/h] |
| $V_{SC}$ | Steepest climb speed | [km/h] |

| | | |
|---|---|---|
| $V_{TD}$ | Touch-down speed | [km/h] |
| $V_{W_{LO}}$ | Wind speed at lift-off | [km/h] |
| $V_{W_{TD}}$ | Wind speed at touch-down | [km/h] |
| $V_{TD_W}$ | Weight reduce touch-down speed | [km/h] |
| W | Weight | [N] |
| $X_G$ | Center of gravity position | [% MAC] |
| $X_N$ | Neutral point position | [% MAC] |
| $\alpha$ | Angle of attack | [deg] |
| $\beta$ | Angle of sideslip | [deg] |
| $\gamma$ | Climb angle | [deg] |
| $\delta_a$ | Aileron deflection | [deg] |
| $\delta_e$ | Elevator deflection | [deg] |
| $\delta_r$ | Rudder deflection | [deg] |
| $\eta_p$ | Propeller efficiency | [-] |
| $\theta$ | Pitch angle | [deg] |
| $\Theta$ | Temperature | [K] |
| $\lambda$ | Aspect ratio | [-] |
| $\rho_0$ | SSL air density | [kg/$m^3$] |
| $\sigma$ | Ratio between day density and ground standard density | [-] |
| φ | Roll angle | [deg] |
| ψ | Yaw angle | [deg] |

# List of Acronyms

| | |
|---|---|
| A/C | Aircraft |
| AOA | Angle of attack |
| ASL | Above Sea Level |
| BHP | Brake Horsepower |
| CAS | Calibrated Airspeed |
| CG | Center of Gravity |
| CHT | Cylinder Head Temperature |
| CR | Cruise |
| DAer | Department of Aerospace Science and Technology |
| EAS | Equivalent Airspeed |
| EFIS | Electronic Flight Instrument System |
| FTE | Flight Test Engineer |
| FTG | Flight Test Guide |
| FTI | Flight Test Instrumentation |
| GPS | Global Positioning System |
| GS | Ground Speed |
| IAS | Indicated Airspeed |
| LND | Landing |
| MAC | Mean Aerodynimic Chord |
| MCP | Maximum Continuos Power |
| MEMS | Micro Electro Mechanical System |
| MTOW | Maximum Take-Off Weight |
| OAT | Outside Air Temperature |
| ROC | Rate Of Climb |
| RPM | Revolutions Per Minute |
| SEP | Specific excess power |
| SHSS | Steady Heading Side-Slip |
| SSL | Standard Sea Level |
| TAS | True Airspeed |

| | |
|---|---|
| TO | Take-off |
| TP | Test Pilot |
| UL | Ultralight |
| VFR | Visual Flight Rules |

# Chapter 1 – Introduction

## 1.1 Scope

The Department of Aerospace Science and Technology of the Politecnico di Milano (DAER-PoliMI) started a collaboration with Ing. Nando Groppo Srl in 2008. This is a highly valued ultralight aircraft manufacturer located in Mezzana Bigli, a small town close to the city of Pavia, Italy. The company has been founded in 1993 by Nando Groppo who gave his name to the company. Many flight test missions on different UL aircrafts have been executed thanks to this collaboration. During the years some co-operative projects have been pursued involving DAER and Ing. Nando Groppo Srl in the development and certification of the latter products.

The last A/C produced is the G70, whose first version has been manufactured in 2015, the second one in 2016 and the third one, the subject of this thesis, across 2017 and 2018. The last version shares most of its characteristics whit the previous versions but it features some significant modifications, which are well described in chapter 2.2.

The campaign aimed to check the aircraft compliance to the German LTF-UL normative (18). Moreover, a new type of test has been performed in the last part of the campaign in order to evaluate the performance of the aircraft.

## 1.2 Test campaign

The campaign took place between February and May 2018. The first test planned was the one concerning the anemometer calibration, which took a long period due to the different modifications applied in order to reach the desired result. After this fundamental step, aircraft stall speed and stall behavior have been investigated. The other tests, which referred to LTF-UL, have not been performed since the German inspector accepted the ones performed in the last campaign on the latter G70. The last part of the campaign aimed to evaluate the climb

performance of the airplane using a technique which is not the common one usually used: the acceleration test.

All tests have been performed and post-processed by the author in the role of Flight Test Engineer. The test pilot, during the entire campaign, was Simone Quaglietta.

Test points have been executed applying the standard techniques described in the CS23 FTG (4), according to LTF-UL prescriptions. Data have been recorder by hand, especially during the anemometer calibration tests, and by means of the Mnemosine Flight Test Instrumentation. The software employed for the post-processing phase, including the plot of all the graphs, has been developed in MATLAB.

## 1.3 Structure of the thesis

The thesis starts with the description of the test aircraft and of the area where tests have been performed. The following chapter describes the instrumentation employed during the campaign, in terms of sensor features, sample frequencies and main limitations. This chapter includes also the description of the filtering process employed on the data by the author; an example of its functioning is also present.

After this introduction the campaign is presented, with its planning and later there is the main corpus of the work. For each test there is a part concerning the test technique employed, the results and the conclusions. In particular the first part is about the anemometer calibration, which is also discussed in the appendix A at the end of the thesis. The following part is about the stall speed. The last part concerning the certification process describes the stall behavior of the aircraft. The last part of the work introduces and describes a new type of technique used to study the climb performance of the airplane.

# Chapter 2 – Test aircraft and test range

In this chapter, test aircraft and test location are described. Moreover, the differences between the current model and the previous one are presented.

## 2.1 Test aircraft

The test aircraft is the new model of G70, the third of its family: the TRAIL SBS G70. It is an ultralight aircraft designed and built by Ing. Nando Groppo Srl. and it features foldable high-wing, single engine, two side-by-side seats and it is meant for recreational and cross-country flying and non-acrobatic operations. Thanks to its easy handling the G70 is also suitable for pilot basic training.

It presents a light alloy structure, a fixed tricycle landing gear with the front wheel steerable by the rudder pedals. The A/C mounts two fuel tanks in the wings, with a capacity of 50 l each. Elevator trim is controlled via buttons integrated in the stick, instead the flap actuator is controlled via a switch installed on the left side of the instrument panel.

The main landing gear is constituted by a single leaf spring in alloy fixed under the fuselage. The main wheels are equipped with disc brakes, actuated by a hydraulic pump with the control lever positioned in the center console between the pilot and the passenger. The hydraulic circuit of the brakes is provided with a non-return valve operable by the pilot for parking.

Table 2.*1* and *Table 2.2* summarize respectively the main geometric characteristics and limitations of the airplane.

| | |
|---|---|
| Wingspan | 8.92 [m] |
| Length | 6.22 [m] |
| Width | 2.74 [m] |
| Height | 2.32 [m] |
| Wing surface | 10.70 [sm] |
| Wing load | 43.3 [kg/sm] |
| Cabin width | 1.22 [m] |
| Landing gear track | 1.80 [m] |
| MAC | 1200 [mm] |

Table 2.1: G70 geometric characteristics

| | |
|---|---|
| MTOW | 472.5 [kg] |
| Maximum project weight | 600 [kg] |
| Maximum weight of fuel | 72 [kg] |
| Maximum weight of luggage | 40 [kg] |
| Minimum crew weight | 55 [kg] |
| Operating CG range | 24 to 35 % of MAC |
| $V_{FE}$ | 110 [km/h] |
| $V_{NE}$ | 220 [km/h] |
| $V_{NO}$ | 180 [km/h] |
| Ceiling | 15000 [ft] |
| Max/Min load factor | +4/-2 [g] |

Table 2.2: G70 limitations

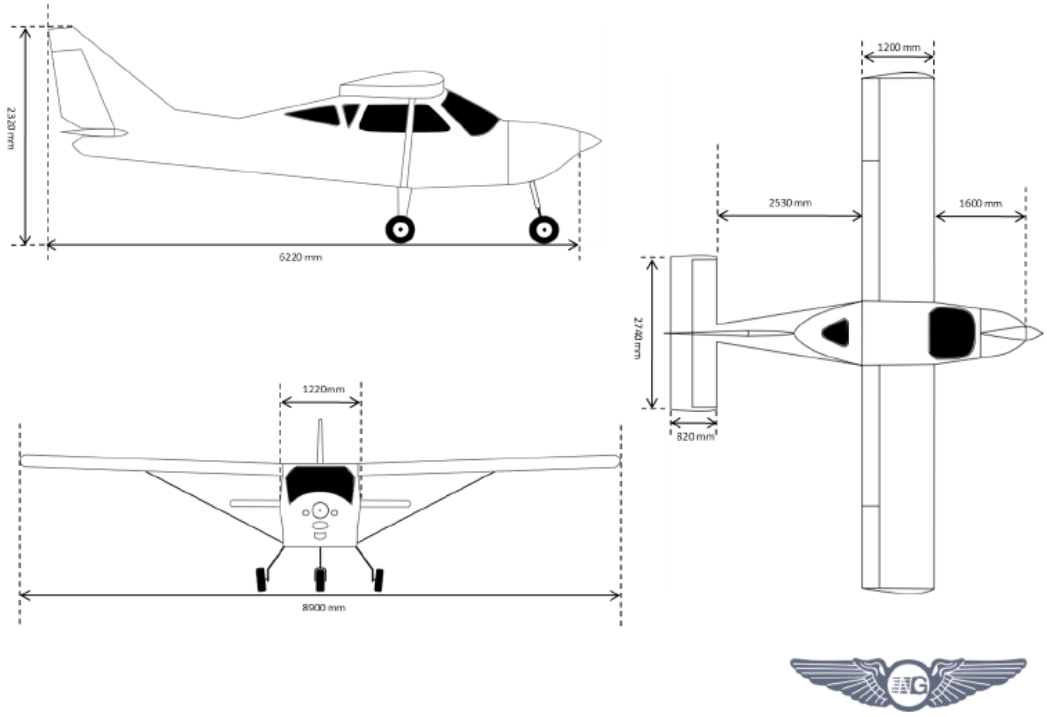


Figure 2.1: G70 three views

Figure 2.2: G70 on the apron

The engine is a Rotax 912ULS, four stroke, four cylinders, able to provide a maximum take-off power of 73.5kW (98.6 Hp) at 5800 rpm. The propeller is the Helix H50F R-TM-18-3 and it presents three blades, fixed pitch, with a diameter of 1.75 m.

The A/C mounts double commands so both seats can be used to pilot. Seats can be adjusted according to pilot size in the longitudinal direction and they are equipped of four-point seat belts. Behind the seats there is the luggage compartment, which can be loaded with a maximum of 40 kg (with rescue system installed).

Cockpit is equipped with the instrumentation shown in *Figure 2.3* and listed in *Table 2.3*.


Figure 2.3: G70 cockpit

| | |
|---|---|
| 1 | Throttle |
| 2 | Fuel pressure indicator |
| 3 | EFIS |
| 4 | Engine parameters |
| 5 | GPS |
| 6 | Mnemosine FTI |
| 7 | Altimeter |
| 8 | VHF radio |
| 9 | Ignition/magnetos switch |
| 10 | Master switch |
| 11 | Beacon switch |
| 12 | Auxiliary fuel pump switch |
| 13 | Elevator trim indicator |
| 14 | Flaps control switch and indicator |
| 15 | Choke |
| 16 | Parking brake valve |

Table 2.3: G70 cockpit description

## 2.2 Comparison with the previous version

As said before this is the third version of G70: the first one has been designed between 2014 and 2015, the second one between 2016 and 2017 and the third one between 2017 and 2018. In the latter version there are few but important modifications:

- Ailerons control:
  - Cables have been substituted with bars, which work in compression, traction and torsion.
- Flaps:
  - They can be now negatively deflected of 5deg at high speeds in order to increase the stability of the A/C.
  - The gap between wing and flap has been closed with a plastic foil in order to improve the aerodynamic. This is helpful to decrease the stall speed as shown in chapter 5.2.4.
- Static pressure probe:
  - In the previous model the static pressure probe was placed in the cabin – even if this condition is not certifiable - due to a high error when placed outside. In this model the total pressure probe has been mounted just under the left wing, instead the static probe has been placed on the fuselage, as shown in *Figure 2.4*. A complete study about the correct position of the static probe has been carried out during the initial phase of the test campaign. The reader can refer to chapter 5.1.

Figure 2.4: Particular of the static pressure probes

## 2.3 Test area

The location for the whole test campaign has been the Aviosuperficie Club Astra, a club located in Mezzana Bigli, a small town near Pavia, Italy. The airstrip is a 900 m, grass, with orientation 02-20. Test area has been limited between ENI refinery, in front of the airstrip for 020-headed take-off and Po River, which is located 2 km south of the airfield. Test phase started in February so thanks to the cold temperatures thermal raisings from the ground have been avoided in the beginning. As spring began the test flights took place in the morning and in the late afternoon in order to avoid turbulences at low altitude. For what concerns VFR sunny days were not a problem, instead cloudy days imposed to reduce test range, especially with regards to altitude, in order to remain in safe VFR conditions, far enough from the cloud ceiling.

## 2.4 Limitations

All tests have been performed in the uncontrolled airspace of class G, with the limitations provided by the Italian regulations for basic ultralights. In particular the altitude is limited to 2500 ft/asl and the visibility has to be at least 5 km and there must be at least 1.5 km of separation from the clouds. So it is clear that the most relevant limitation is due to meteorological issues. In fact, in particular in the beginning of the campaign, there were many delays due to fog and rain. In the middle phase of the campaign, when spring began, weather was characterized by strong winds which added new delays. Despite this the campaign followed its scheduling and it was concluded with success.

# Chapter 3 – Test instrumentation and data filtering

This chapter describes all the instrumentation which make up the Flight Test Instrumentation for the campaign. The set of sensors is suitable to provide a time history of all the parameters needed to perform a fully satisfactory analysis of the flights.

Most of the data required a filtering operation in order to have them readable for the post processing analysis; filtering will be discussed in the last part of this chapter.

## 3.1 Mnemosine Mk-V

Flight test instrumentation is the Mnemosine Mk-V, fifth generation of the FTI developed at Politecnico di Milano, at the Department of Aerospace Engineering, by Professor Alberto Rolando (13). This FTI is based on a central unit, shown in *Figure 3.1*, connected with all the sensors, able to record 35 parameters on a removable SD card. The sensor suite includes:

- Inertial measurement unit (XSENS);
- GPS unit (GPS);
- Flight control position sensors (ADC);
- Air data sensors (ADS);
- Stick force sensor.

The FTI involves also a dashboard to switch on and off the data registration and a kneepad, which displays immediately some parameters chosen by the user. The kneepad also permits to mark the time when a particular event occurs, such as a trim shot, and besides it can be marked when a test phase starts and ends.

*Table 3.1* summarizes the sample frequencies of each FTI unit.

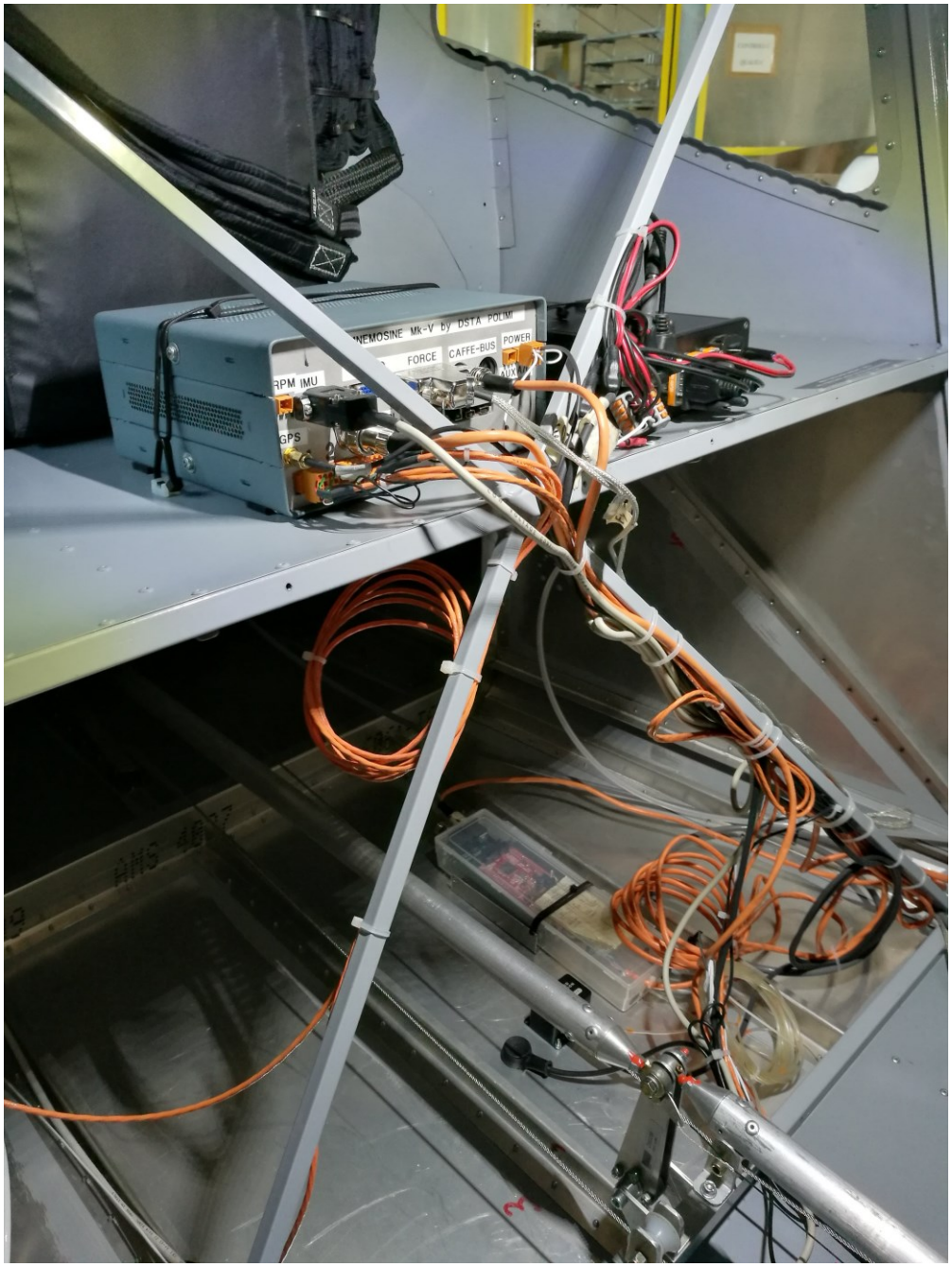


Figure 3.1: Mnemosine MK-V mounted in the G70 luggage compartment

| Sensor type | Frequency [Hz] |
|---|---|
| XSENS | 50 |
| GPS | 2 |
| ADC | 10 |
| ADS | 10 |
| Stick force | 10 |

Table 3.1: Sample frequencies

For a complete overview of the FTI, the reader might refer to (1).

A Pitot Boom bought by the Politecnico di Milano DAer in May 2017 completes the FTI; its details are given in chapter 3.1.4.

### 3.1.1 Inertial measurement unit

The inertial measurement unit features 3 MEMS gyro axes, 3 MEMS accelerometer axes, barometer, 3D magnetometer, GPS and odometer interface. The integrated Kalman filter based data fusion provides secured attitude even at lost of the aiding data. The outputs are:

- Acceleration along the three axis;
- Angular velocity along the three axis;
- Euler angles.

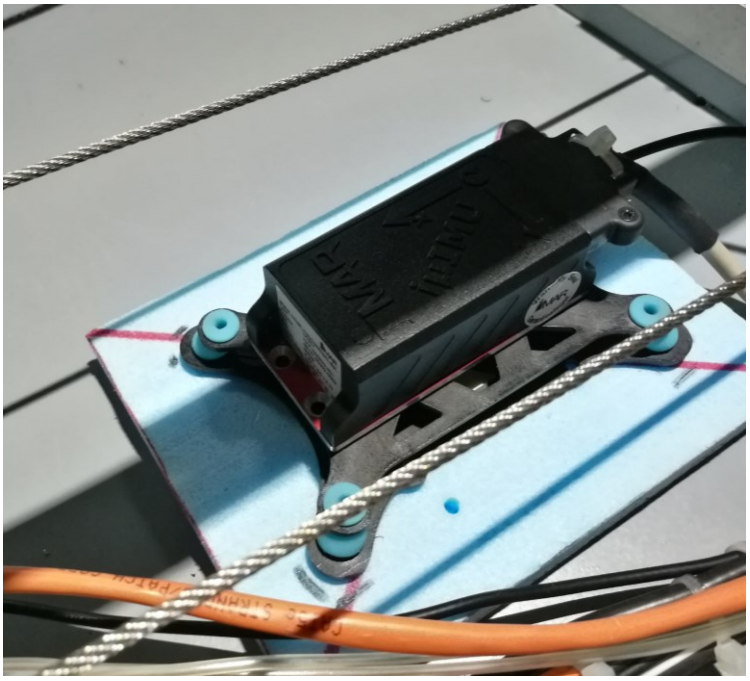

Figure 3.2: FTI Inertial Measurement Unit

### 3.1.2 GPS unit

The GPS module is used both as positioning sensor and as time source. The GPS installed on the Mnemosine Mk-V is the LEA-6N, a standalone positioning module that combines an extensive array of features with flexible connectivity options. LEA-6N supports GPS, GLONASS and QZSS modules.

### 3.1.3 Flight control position sensors

Ailerons, flaps, elevator and rudder position comes from a set of LX-PA-3.8 wire potentiometer. The moving part is attached to the connection between bar and surface, while the body is attached to the cabin floor. The cable movement pulls a spring connected to a potentiometer. The cable spring maintains a constant pull back tension on the cable. These sensors guarantee a good level of safety, since the wire might be broken if they create an obstacle for the deflection of the control surface. *Figure 3.3* presents an example of potentiometer mounted on the A/C.

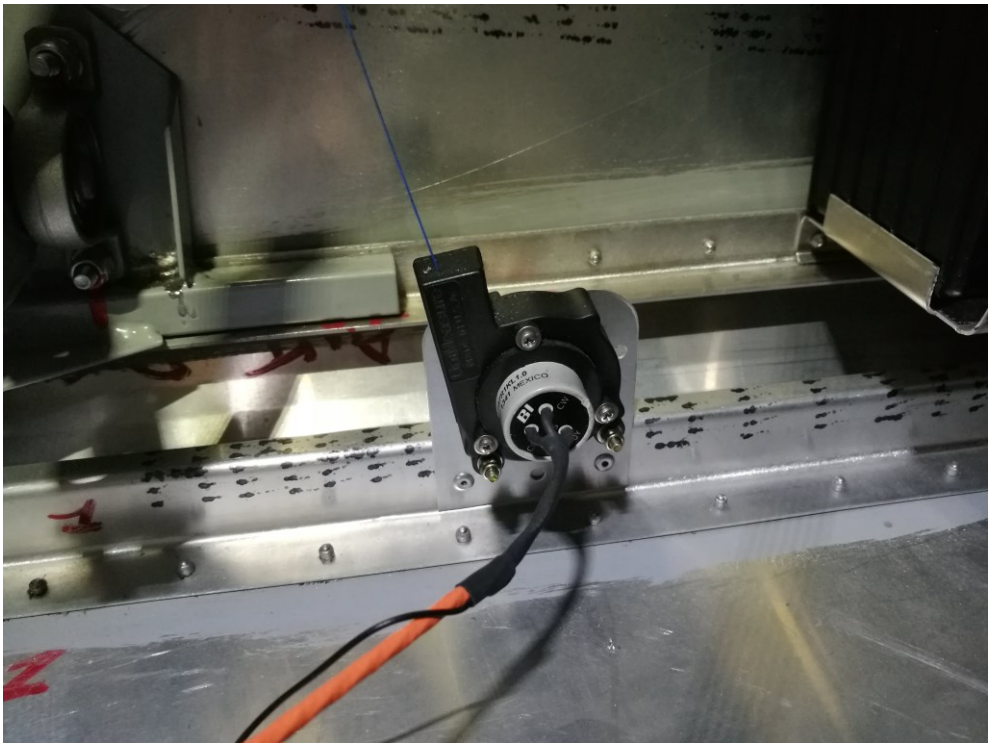

Figure 3.3: Aileron potentiometer

### 3.1.4 Air data module

All the air data are collected thanks to a 100400 Mini Airdata Boom, whose sketch and components are presented in *Figure 3.4*. In particular the boom hosts a static probe, a total pressure one, an angle of attack sensor and an angle of sideslip one. The entire air data module is composed by an Olimex STM32-H107, two pressure transducers (static and dynamic air pressure), one resistance to detect the temperature and an analogue conditioning module for wind angle measures. This module is the only one stored outside the main FTI unit in order to avoid too long linkages between the probes and the transducers.

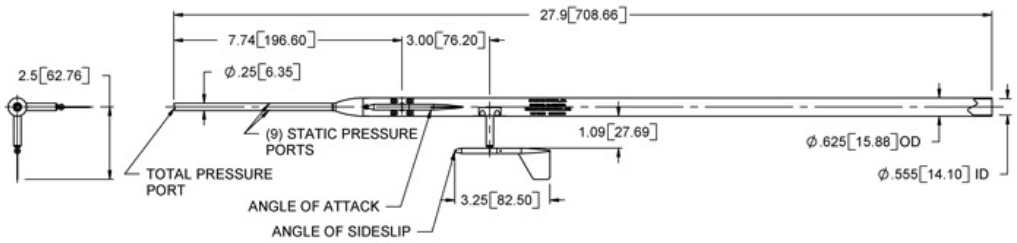


Figure 3.4: Air data boom sketch

### 3.1.5 Stick force sensor

The Futek MU300, a small 3D load cell, acquires the stick force. This cell is coupled with a HX711 load cell amplifier to get measurable data. The load cell senses the stick force in both directions. The sensor is mounted as shown in the following picture.


Figure 3.5: Instrumented control stick

### 3.1.6 Dashboard and kneepad

The kneepad is composed by an LCD screen and three commands: one switch, one button and one knob, as shown in *Figure 3.6*. Switch is used to open and close the TOP, in order to visualize on the mission time line the beginning and the end of each test phase. The button is useful to mark a specific event on the time line. Finally, the knob is used to switch from one page of the screen to another. The screen allows the FTE to have in sight some real-time parameters.


Figure 3.6: Mnemosine Mk-V kneepad

The dashboard has been installed just in front of the head of the FTE so that an easy access was possible. It permits to turn on and off the whole FTI. In particular it has five switches:

- MASTER: to turn on and off the system;
- TELEMETRY: to control the power of the telemetry transceiver;
- AUX: to supply the FTI from an external power supply;
- A/C: to supply the FTI directly from the aircraft electrical system;

- RECORD: to start and stop data recording.

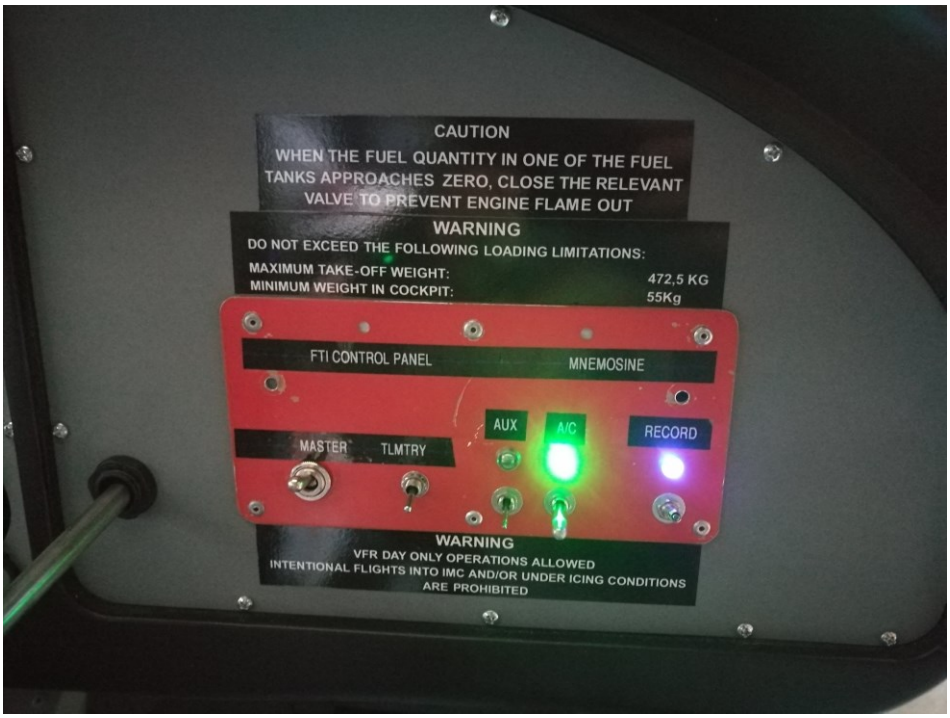


Figure 3.7: FTI dashboard

# 3.2 Data filtering

Data from FTI have been filtered with a Butterworth filter using the function "filtfilt" already existing in Matlab environment. This function processes the data forwards and backwards and compensates the delay introduced by the filtering. Butterworth filter is implemented in Matlab with the following function:

$$[b,a] = \text{butter}(\text{order}, \omega_n)$$

Where:

- b and a: numerator and the denominator coefficients of the filter transfer function, as output;
- order: filter order;
- $\omega_n$: normalized cut-off frequency, its formula is: $\omega_n = \frac{f_c}{f_s/2}$

Sample frequencies are the one reported in *Table 3.1*, while cut-off frequency $f_c$ has been set to 1 Hz for all the data. This value allows to analyze all the data without losing information and, at the same time, cut off all the noise coming from structural vibration of the aircraft. With higher frequencies the time history if dirty of noise oscillations, while with lower frequencies there is the risk to lose information. Filter order has been chosen equal to four. This value reaches all the data peaks, making the filtered time history sufficiently accurate.

An example of filtering is now presented, the XSENS data of flight 01.0304 have been used for this example. As mentioned before XSENS channel includes the following data: Euler angles, angular velocities and axial accelerations. The data input, for the above said formula, have been the following:

- $f_c = 1$;
- $order = 4$;
- $f_s = 50$.

*Figure 3.8* represents the magnitude function of the obtained filter. Since the filter has been applied using a zero-delay filtering technique, the phase plot can be omitted.

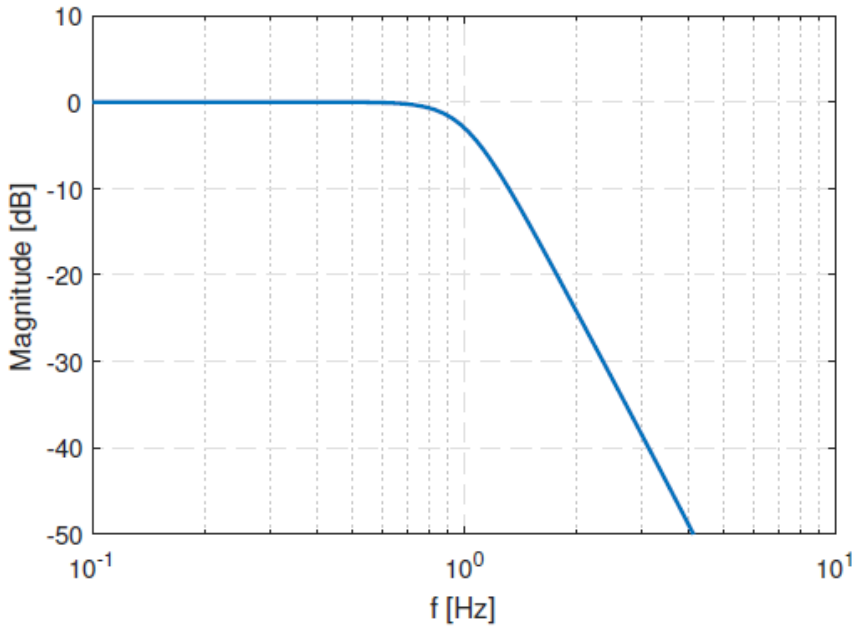


Figure 3.8: Magnitude filter

*Figure 3.9*, *Figure 3.10* and *Figure 3.11* show the comparison between the raw and the filtered signal for each of the channel of the XSENS data set. Thanks to these images it is clear the good result given by the filtering action.

Moreover, it is interesting to notice that the Euler angles do not need any type of filtering action since raw and filtered data coincides.

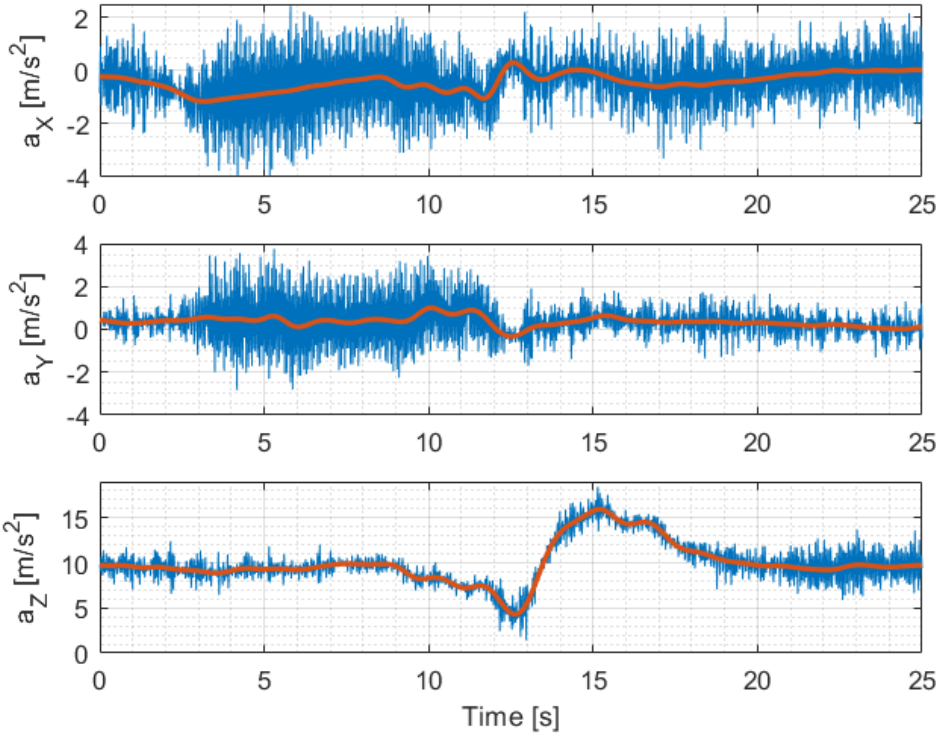


Figure 3.9: Raw data and filtered data - Acceleration signal

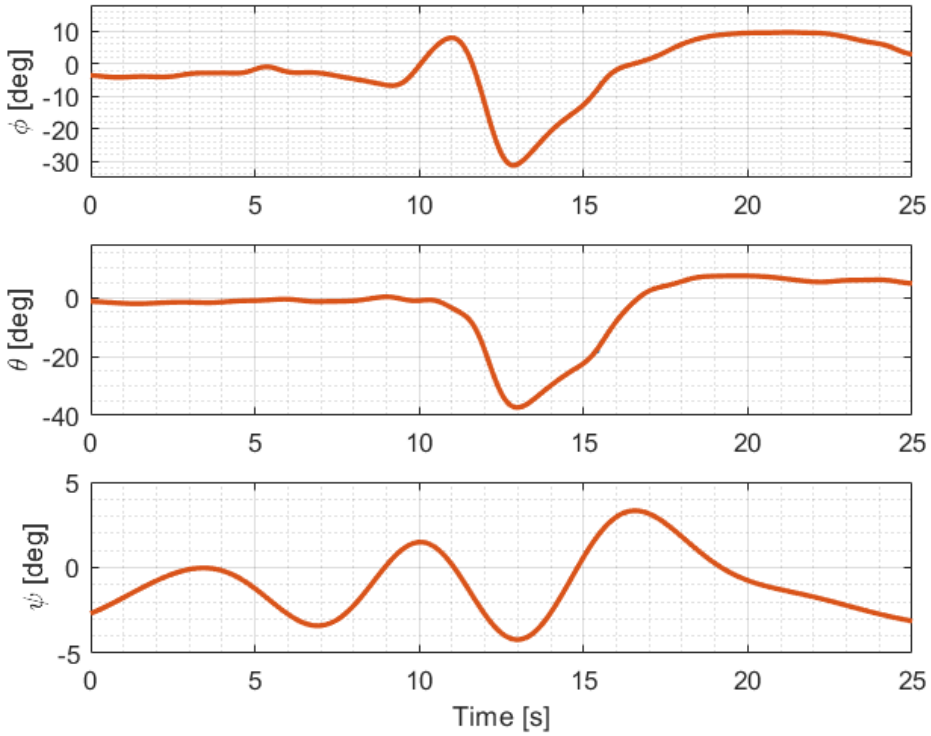


Figure 3.10: Raw data and filtered data - Euler angles channel

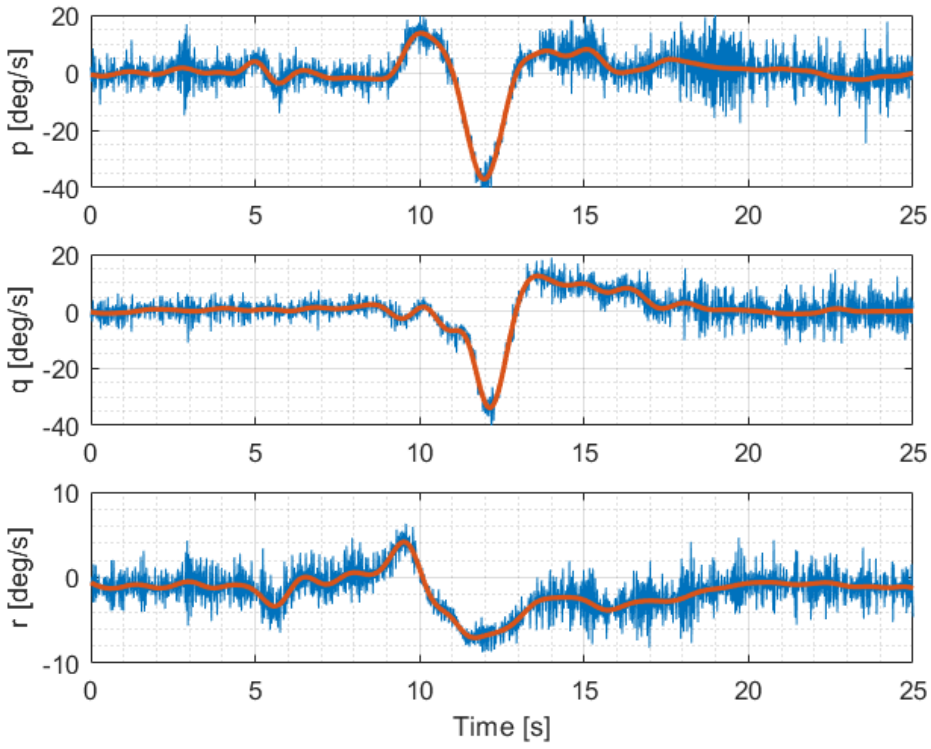


Figure 3.11: Raw data and filtered data - Angular velocities channel

# Chapter 4 – Test campaign preparation

The campaign started with the analysis of the regulatory background, which will be fully explained in the following chapter. After this, the first main goal was to accomplish the normative about the air data calibration. Only after succeeding in this crucial point the campaign could continue. All tests have been performed by the author in the role of flight test engineer and by Simone Quaglietta as test pilot.

## 4.1 Regulatory background

Ing. Nando Groppo Srl wants to certify its aircrafts following the German law. In particular the G70 has to accomplish the LTF-UL regulation. In order to understand this decision a digression about UL aircrafts is needed.

In Italy UL aircrafts regulation is contained in the Legge del 25 marzo 1985, n. 106 (2) and in the Decreto del Presidente della Repubblica, 9 luglio 2010, n. 133 (DPR 133) (3). In particular, UL airplanes are divided in two categories: basic and advanced. Besides the DPR 133 defines all the test points that must be accomplished in order to certify the A/C according to the Italian law. In Germany, instead, the DULV (German Ultralight Association) is responsible of the UL certification with the LTF-UL as well as AeCI (Aero Club Italia) is responsible to release the certification in Italy.

The main difference between the Italian and the German regulation is that the latter is more detailed and structured than the former. Besides an accomplishment of the LTF-UL guarantees an accomplishment of the DPR 133, while the opposite is not true.

So it is now clearer the decision made by Ing. Nando Groppo Srl to follow the German regulation. It must be said also that this decision is appreciated abroad in particular, as clear, in Germany.

## 4.2 Test campaign planning

The test campaign planning is presented in the following table. It can be noticed that the majority of the flights lasted about 20 - 25 minutes. This fact allows to consider the A/C weight constant during flight tests because the fuel consumption is not relevant.

Between flight number 5 and 6 there was a long break due to the repaint of the A/C and small changes in the cockpit instrumentation. Instead, another break is present after flight number 11 because the majority of the aircrafts have been dismounted and brought to Germany because of the Aero Friedrichshafen fair.

| Flight ID | Progressive number | Date | Duration [min] | Test items |
|---|---|---|---|---|
| 01.1302 | 1 | 13/02/2018 | 50 | Air data calibration (CR) |
| 01.1502 | 2 | 15/02/2018 | 45 | Air data calibration (CR) |
| 02.1502 | 3 | 15/02/2018 | 48 | Air data calibration (CR) |
| 03.1502 | 4 | 15/02/2018 | 39 | Air data calibration (CR) |
| 01.1602 | 5 | 16/02/2018 | 38 | Air data calibration (CR) |
| 01.3103 | 6 | 31/03/2018 | 45 | Air data calibration (CR) |
| 02.3103 | 7 | 31/03/2018 | 40 | Air data calibration (CR) |
| 03.3103 | 8 | 31/03/2018 | 48 | Air data calibration (CR) |
| 04.3103 | 9 | 31/03/2018 | 50 | Air data calibration (CR) |

| | | | | |
|---|---|---|---|---|
| 05.3103 | 10 | 31/03/2018 | 35 | Air data calibration (CR) |
| 01.0304 | 11 | 03/04/2018 | 25 | Stall speed determination (CR – TO - LND) |
| 01.2605 | 12 | 26/05/2018 | 45 | - Air data calibration (LND)<br>- Stall test (CG forward)<br>- Acceleration test |
| 02.2605 | 13 | 26/05/2018 | 25 | - Stall test (CG backward)<br>- Acceleration test |

Table 4.1: Test campaign planning

Total flights: 13.

Flight hours: almost 9 hours.

# Chapter 5 – Certification testing

This chapter fully describes the tests performed by the author to complete the certification phase of the airplane. The reader might refer to (14), (15) and (16).

## 5.1 Air data calibration

### 5.1.1 Introduction

This part is one of the most important phases in a test campaign and, as can be seen from the planning, it took a long period and many hours of flight. In fact it is mandatory to have a reliable speed indication onboard in order to keep the A/C far enough from stall speed and from maximum speed.

Anemometer calibration has the purpose to measure and mitigate the error acting on the static probe. This error is due to the pressure distribution along the fuselage (position error). The goal of this test is to identify the better place for the static port in order to minimize the error.

In particular, in the previous model of G70 the air data calibration result was completely unacceptable because of the too high error of the static probe according to the limits imposed by LTF-UL. The solution adopted was to move the static probe inside the cabin but this condition is not certifiable.

In order to overhaul this fundamental phase, many hours have been spent onboard to test different positions of the static probe. Thanks to this, starting from the initial configuration - pitot tube installed under the left wing of the A/C - shown in *Figure 5.1*, the final and definitive configuration has been found: the total pressure probe under the left wing as shown in *Figure 5.2*, and the static pressure probes on the fuselage as shown in *Figure 5.3* and *Figure 5.4*.

Figure 5.1: Initial configuration – Pitot tube

Figure 5.2: Final configuration – Particular of the total pressure tube

Figure 5.3: Final configuration – Particular of the static pressure probes

Figure 5.4: Enlargement of the static pressure probes

## 5.1.2 Test objectives

LTF-UL 1323 states that the air-speed indicating system must be calibrated to indicate true air-speed at sea-level in standard atmosphere with a maximum pitot static error not exceeding ± 6 km/h or ± 5% whichever is greater, throughout the following speed range:

- 1.2 $V_S$ to $V_{NE}$ with flaps retracted
- 1.2 $V_{S0}$ to $V_{FE}$ with flaps fully extracted

The FTI pitot boom does not have any limitation of error according to LTF-UL, but it is desirable that pitot IAS is reliable for almost all the flight tests.

## 5.1.3 Test execution

The procedure utilized for anemometer calibration is the GPS-PEC (Position Error Calibration) described in (8). The error is obtained with a comparison between the IAS read on the anemometer onboard, and TAS, which is identified with the GPS. Since the GPS can only measure GS, it is necessary to identify wind speed and wind direction in order to obtain TAS. The identification is done flying three legs at the same IAS with a heading significantly different among them. So three equations in three unknowns can be solved giving wind speed, wind direction and TAS. A graphical representation of the wind triangles is given in *Figure 5.5*.

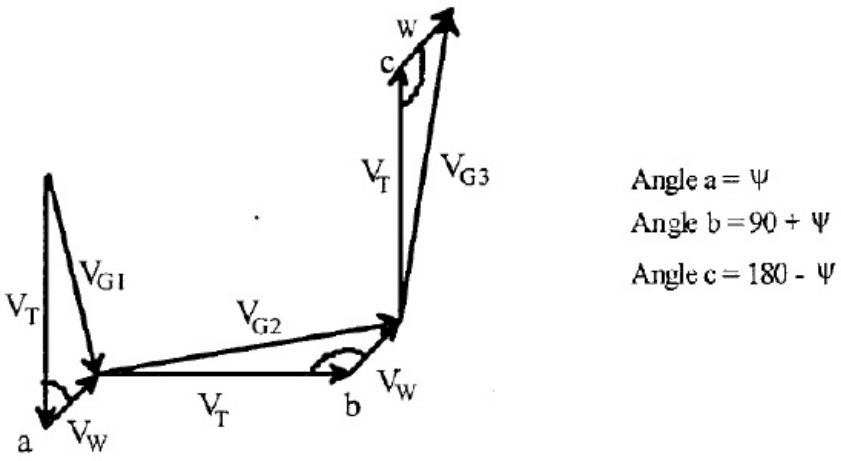


Figure 5.5: Wind triangles

All calibration tests have been performed with four legs instead of three: this brings a more reliable result because there is a system with three unknowns and four equations, which is solved with the least square method.

There are other two important data in order to correctly identify the pressure error: altitude and OAT. In particular, the author and the TP have seen how a little variation of the OAT can bring significantly different results.

Finally thanks to the following equation, CAS is obtained from TAS:

$$EAS = TAS * \sqrt{\frac{day\ density}{standard\ density}}$$

$$CAS = EAS$$

It must be underlined that for the speed and altitude range the assumption EAS=CAS is always more than reliable.

### 5.1.4 Test results

The firsts flights were characterized by unacceptable errors: many attempts have been performed in order to overcome the bad results obtained. Even if this slowed down the entire test campaign, the fact of thinking about new and better solutions improved both the pilot and the author experience in the experimental field.

A complete discussion of all the tests performed is present in Appendix A - Air data calibration.

As mentioned before, after many attempts, the final configuration has been found in the flight 05.3103: the total pressure probe has to be mounted under the left wing taking care of its correct inclination with respect to the one of the aircraft and the static probes on the fuselage of the A/C.

*Figure 5.6* and *Figure 5.7* show the results for the CR configuration.

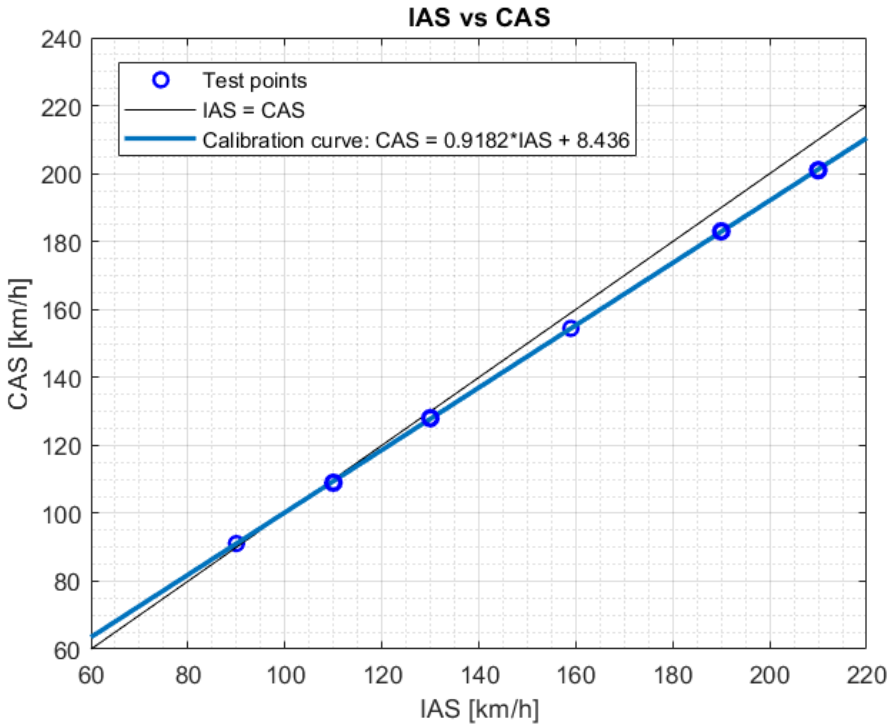


Figure 5.6: IAS vs CAS - CR configuration - flight 05.3103

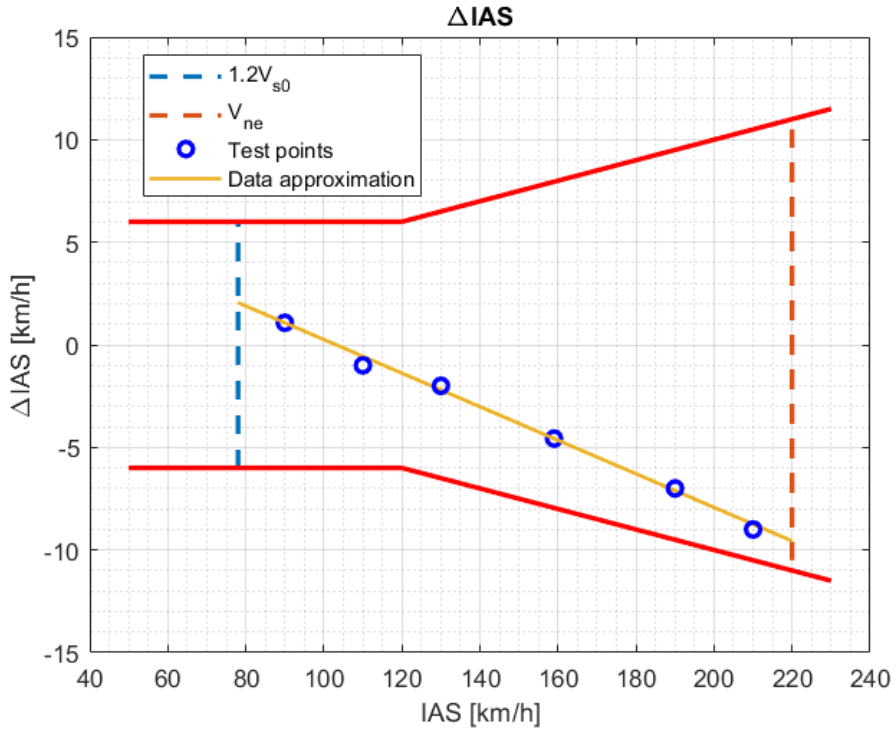


Figure 5.7: IAS error - CR configuration - flight 05.3103

Specifically, from *Figure 5.6*, it can be noticed that near stall speed, IAS is smaller than CAS. This condition is considered secure: in fact the pilot, thanks to the underestimation of the speed, keeps the A/C far enough from the stall condition.

In *Figure 5.7* the red lines represents the error limits accepted by the LTF-UL, instead the green line is the linear approximation of the test points (IAS error versus IAS). It is clear how at low speeds, in particular between 80 and 115 km/h, the error is almost null. Instead, at higher speeds, the error increases but it remains in the limits imposed by the certification.

The following pictures present the results for the landing configuration.

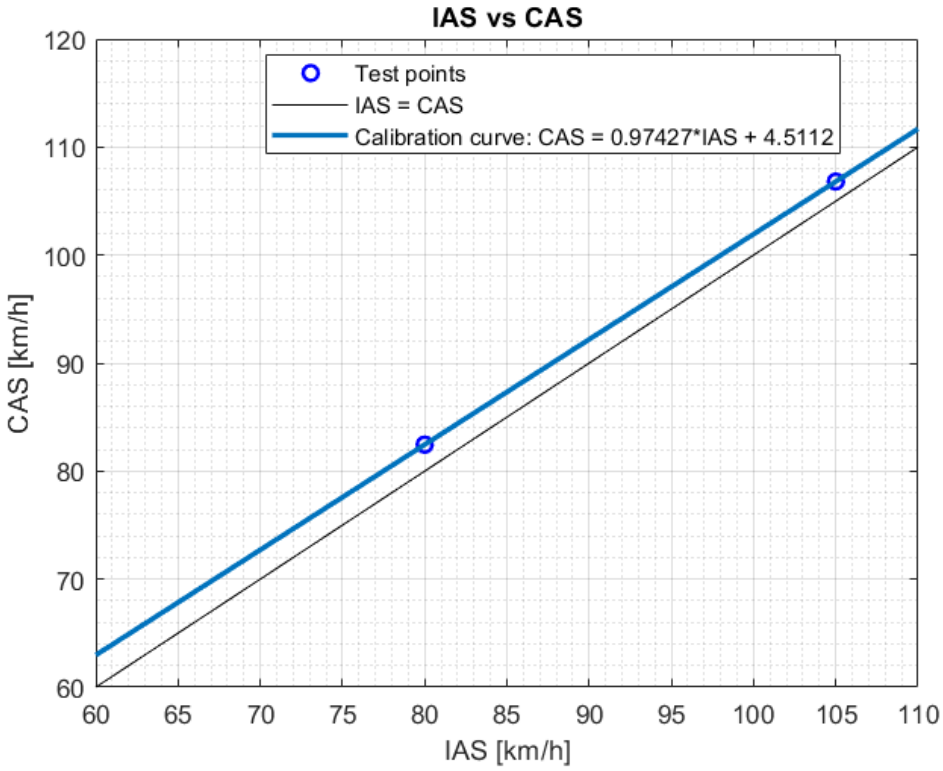


Figure 5.8: IAS vs CAS - LND configuration - flight 01.2605

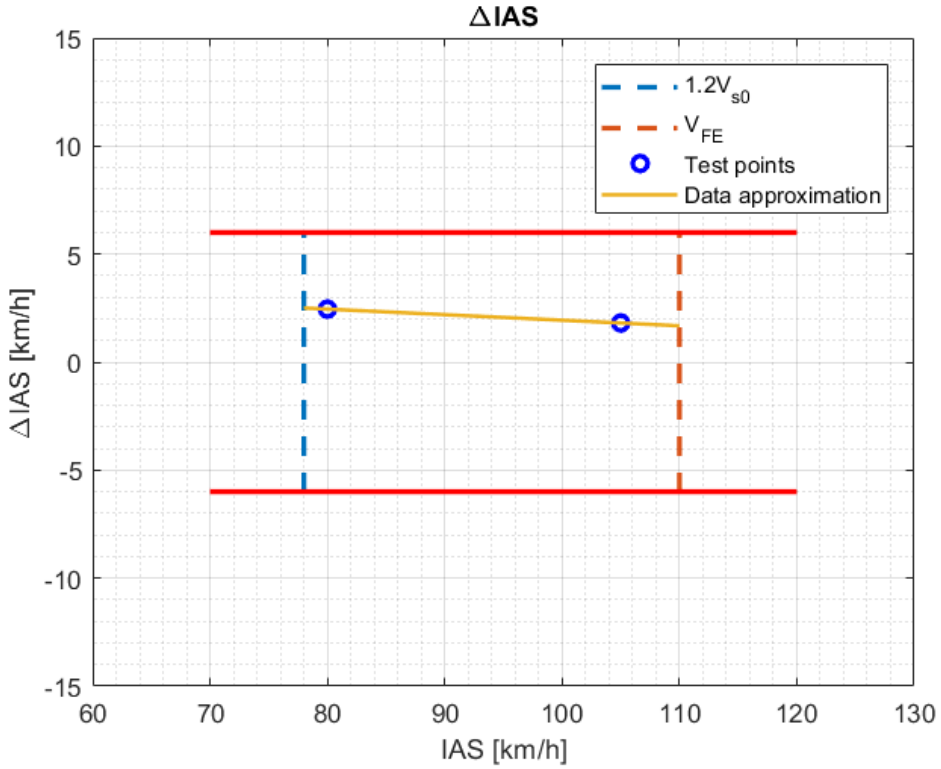


Figure 5.9: IAS error - LND configuration - flight 01.2605

From *Figure 5.8* it can be noticed that the calibration line is shifted of an almost constant quantity above the IAS equal to CAS line. This fact suggests that in this configuration the error is almost constant through the speed envelope. This behavior is different from the one in CR configuration: in fact in that case the error has a linear trend and it increases, in magnitude, as the speed increase. The proof of this can be found in *Figure 5.9*.

In this graph the error at 80 km/h is about 2.5 km/h, while at 105 km/h it is of 2 km/h. So, in conclusion, it can be said that the position error in LND configuration is constant and its value is considered acceptable according to the normative.

### 5.1.5 Conclusions

The second model of G70 did not satisfied the requisites to pass this test. The current version, instead, thanks to an in-depth study of the problem and to appropriate modifications, satisfies the requisites in both configurations and results certifiable under the aspect of the anemometer calibration. Moreover, as it is clear, this is an important and fundamental step throughout the certification process.

## 5.2 Stall speed determination

### 5.2.1 Introduction

The stall speed determination test has been performed in three configurations – CR, TO and LND – and with two different positions of the center of gravity: in the most permitted advanced point and in the most backward point.

Before performing these tests it is difficult to predict the behavior of the A/C since many factors influence the stall speed. However thanks to the new modification brought to the flaps, described in 2.2, a lower stall speed was forecast with respect to the former G70. It useful to underline that only stall speed will be discussed in this chapter. The stall behavior of the A/C will be described in chapter 5.3.

### 5.2.2 Test objectives

LTF-UL in paragraph 49 describes two types of stalling speed:

- $V_{S0}$ is the stall speed, if obtainable or the minimum steady speed, in km/h (CAS), at which the airplane is controllable with the engine at idle (throttle closed) or shut down.

  The A/C must be in LND configuration and the weight must be equivalent to the maximum weight
- $V_{S1}$ is the stall speed (CAS), if obtainable or the minimum steady speed, with the engine idling or shut down.

The A/C is in the condition existing in the test in which $V_{S1}$ is being used and mass must be equivalent to maximum weight.

According to this normative $V_{S0}$ must not exceed 65 km/h and, as described in LTF-UL 201, the standard deceleration at which stall speed has to be determined is 2 km/h/s. Moreover, this paragraph describes how to identify the stall: it is shown by an uncontrollable downward or side-ward pitching movement of the airplane or until the control reaches the stop.

### 5.2.3 Test execution

In order to obtain the stall speed at the prescribed deceleration, at least two test points have to be performed in each test. Usually the first point is characterized by a low deceleration, while the second one has a major deceleration value.

Moreover, wind effects must be as low as possible. To do that, all tests were performed on a trajectory which was perpendicular to wind direction. The detailed procedure is the following:

1. Level the A/C at 1500 ft
2. Trim the A/C at about 90 km/h, in the desired configuration
3. Set the engine in IDLE
4. Pull the stick until a stall is produced, recognized by a sudden pitch or roll brake or by the elevator maximum deflection
5. Regain the normal attitude
6. Trim for the following test point
7. Repeat the procedure with a different deceleration

Stall speed tests have been performed in flights 01.2605 and 02.2605. In both flights, tests have been performed three times with three different A/C configurations, namely: cruise, take-off and land configuration.

The first issue is to identify the stall nature, whether aerodynamic or for maximum elevator deflection. In order to identify the correct nature of each stall, in the post-processing phase, is checked the presence of a pitch or roll brake before the elevator reaches its mechanical limit. Moreover, if the elevator does not reach the limit and there is no evidence of a break, the test point has to be considered not valid.

The stall speed is the calibrated reduced speed with respect to the standard weight of 472.5 kg. The reduced calibrated speed is obtained with the following equation:

$$V_{S_W} = V_S \sqrt{\frac{W_S}{W_T}}$$

It must be underlined that this formula gives an estimate of the stall speed at the certification weight of 472.5 kg. Stall speed at the deceleration imposed by the normative is found with a linear regression among the deceleration-reduced stall speed points.

### 5.2.4 Test results

All stalls occurred with an aerodynamic break and after reaching the limit of the elevator stick, so all test points have been considered valid.

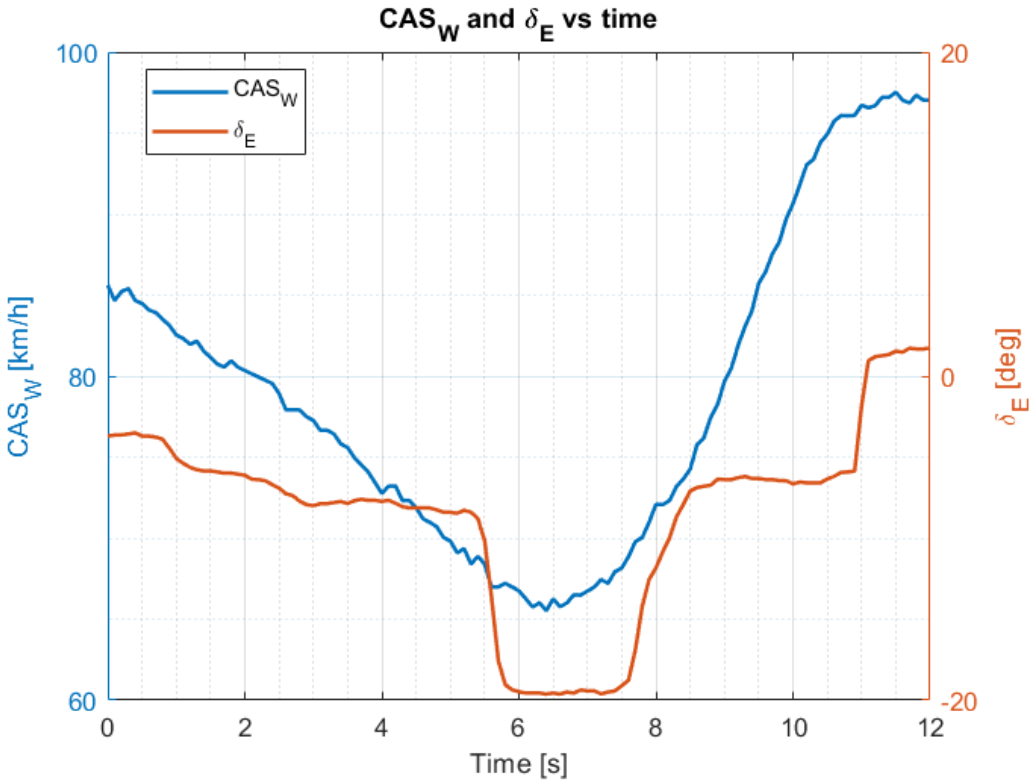


Figure 5.10: Speed and elevator deflection during a stall

*Figure 5.10* shows a typical elevator deflection trend during a stall test. It can be noticed that the elevator reaches its maximum deflection and the pilot keeps it fixed for almost two seconds.

The stall test performed in flight 01.2605 was characterized by a forward CG position, while in flight 02.2605 the CG was in a backward position. To achieve the two different CG positions, two ballasts of 12.5 kg each have been used. In the first flight the ballasts were put just before the pedals, as shown in *Figure 5.11*, instead

in the second flight they were put one behind the passenger seat and the other behind the pilot seat, in particular on the hatbox, as shown in *Figure 5.12* and *Figure 5.13*.

Figure 5.11: Two ballasts behind the pedals

Figure 5.12: Ballast on the hatbox

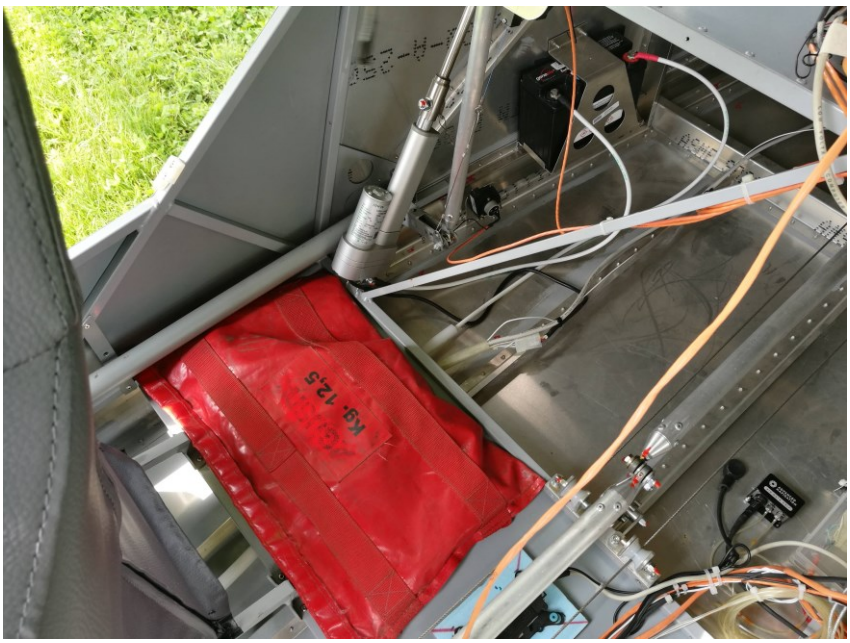

Figure 5.13: Ballast behind passenger seat

Now the graphs of each CG and A/C configurations will be presented. Typically the stall speed with the CG in the forward position is higher than the one with the CG in the backward position. Because of this, the speed certification has to be verified in the most advanced position of the center of gravity.

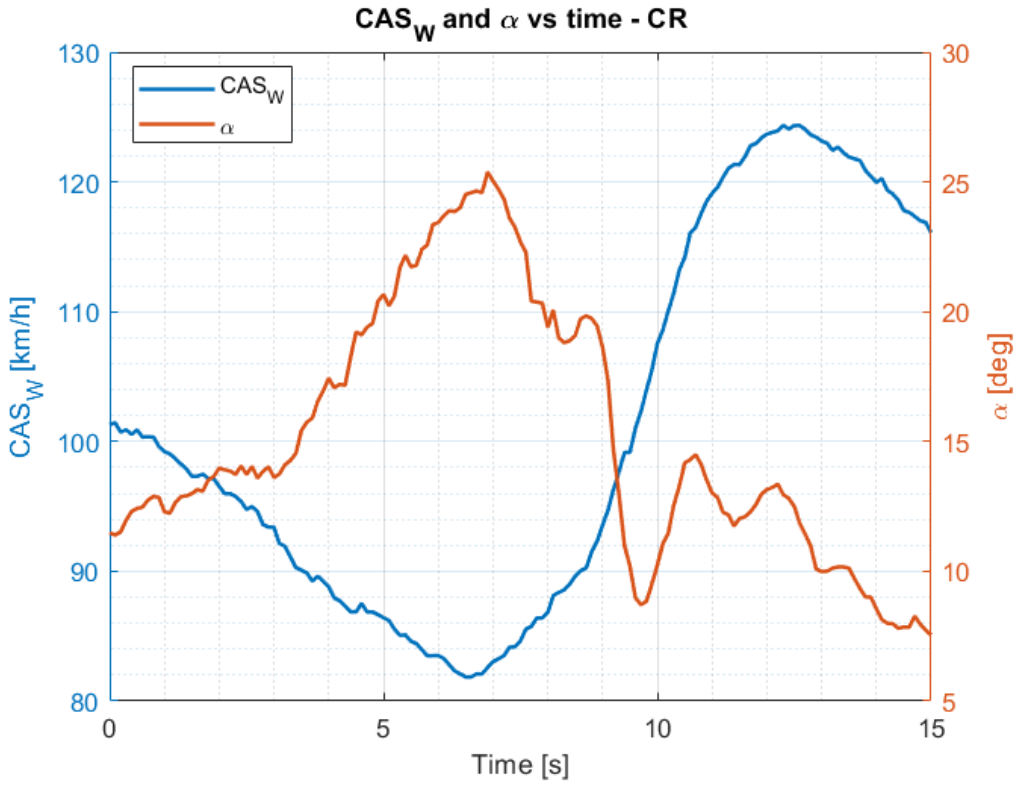


Figure 5.14: Reduced CAS and alpha - CR

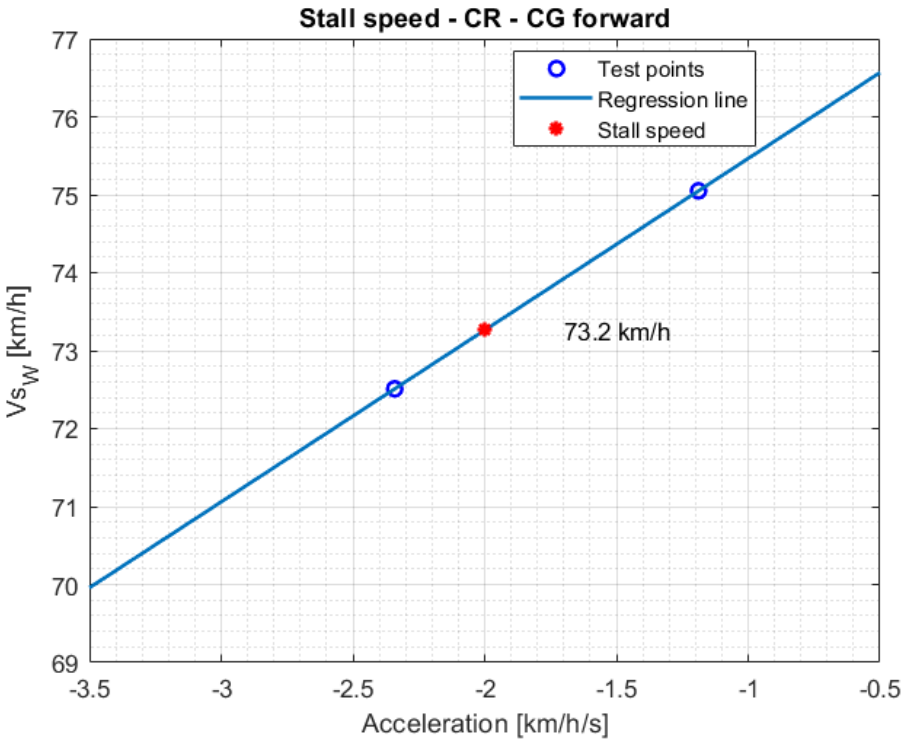


Figure 5.15: Stall speed - CR - CG forward

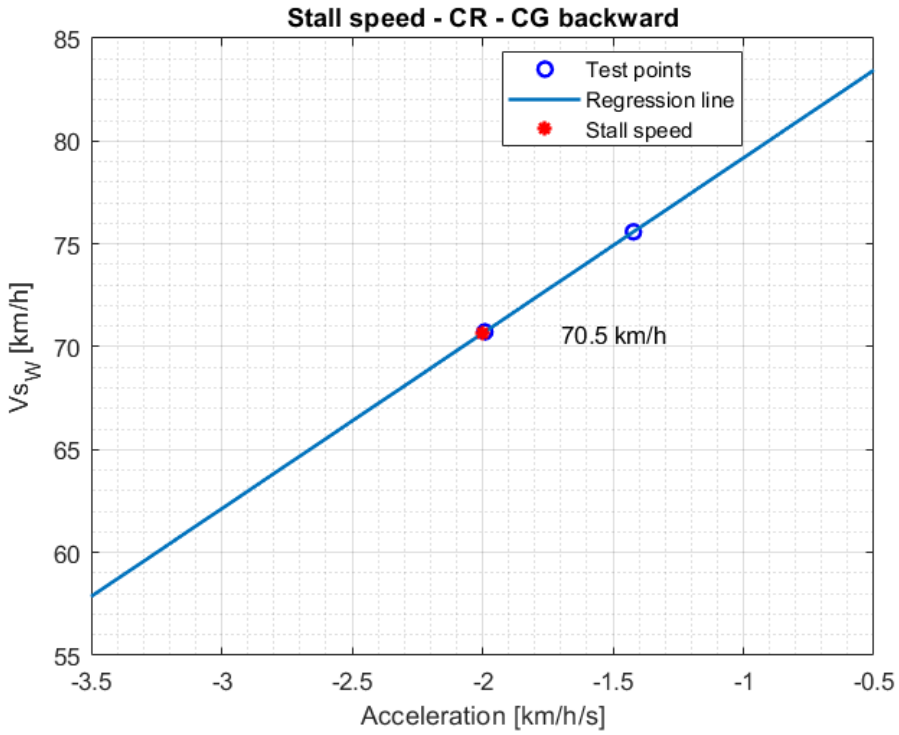


Figure 5.16: Stall speed - CR - CG backward

*Figure 5.14* represents the trend of the reduced airspeed and of the angle of attack during a stall in CR configuration. It can be noticed that the angle of attack increases of 15 degrees during the pitching up maneuver. At the stall the AOA suddenly decreases reaching its minimum.

The other two graphs indicate the weight-reduced stall speed and, as mentioned before, the one with CG forward is greater than the one with CG backward.

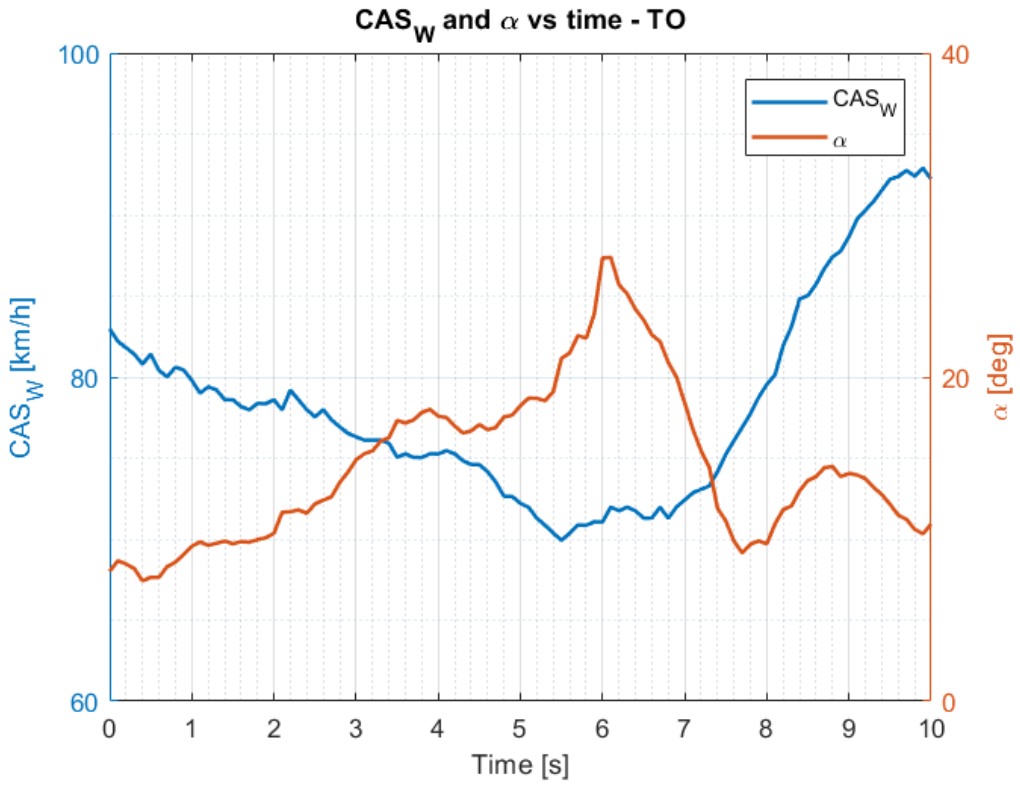


Figure 5.17: Reduced CAS and alpha - TO

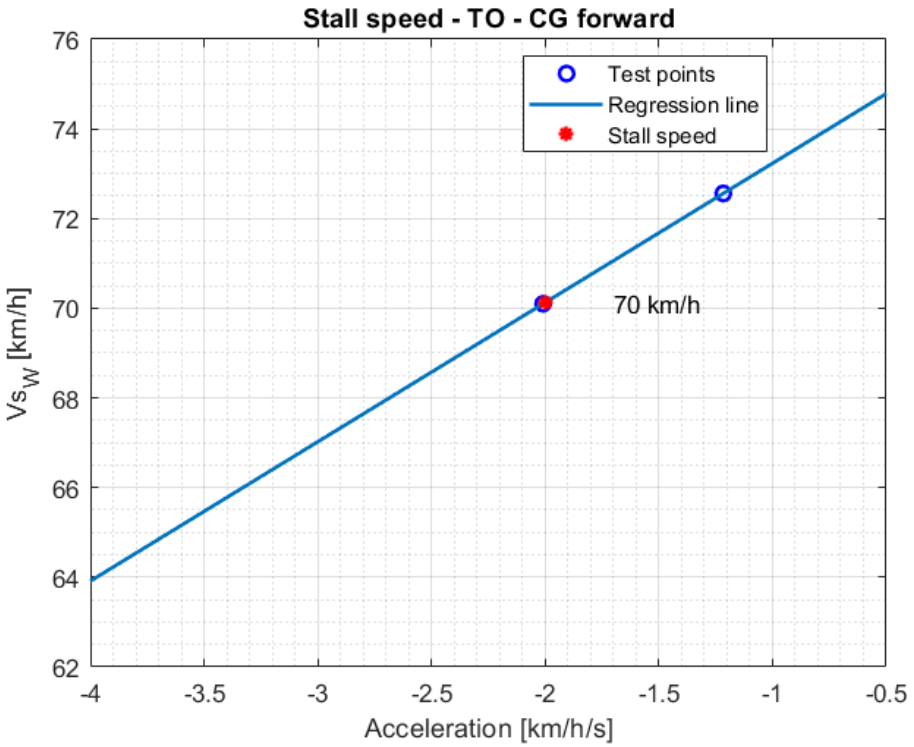


Figure 5.18: Stall speed - TO - CG forward

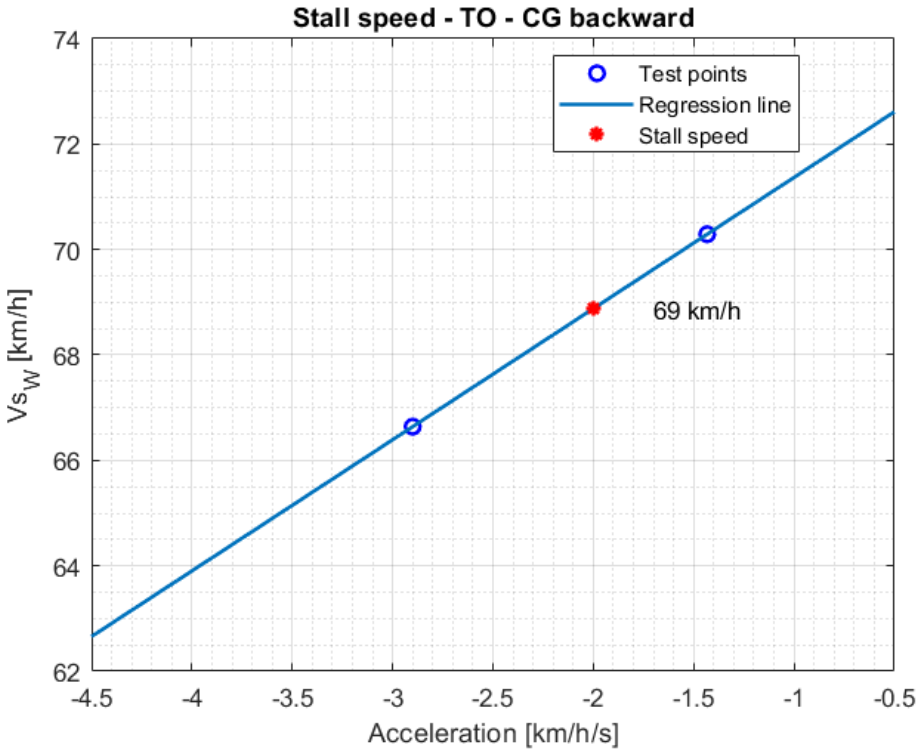


Figure 5.19: Stall speed - TO - CG backward

*Figure 5.17* represents weight-reduced stall speed and angle of attack in TO configuration. It can be noticed that the maximum of the AOA is increased with respect to the one in CR configuration. This underlines the lift increasing action of the flaps, even if they are deflected of only few degrees. From *Figure 5.18* and *Figure 5.19* it can be seen that, as forecast, the stall speed in TO configuration is slightly lower than the previous.

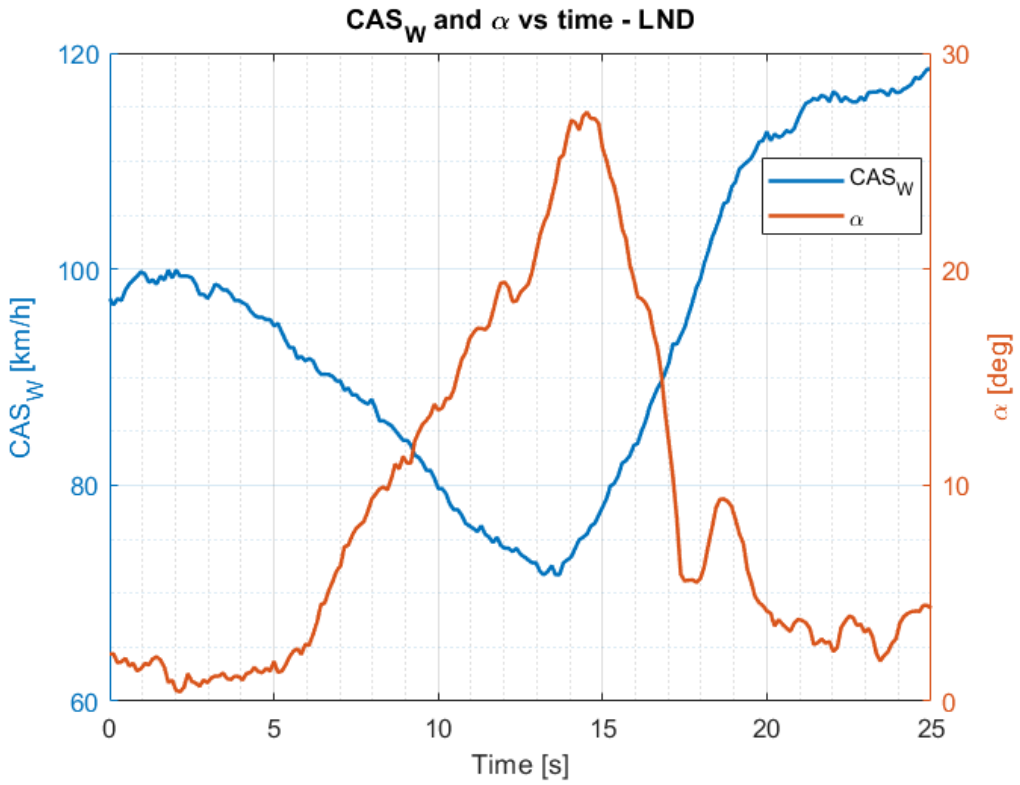


Figure 5.20: Reduced CAS and alpha - LND

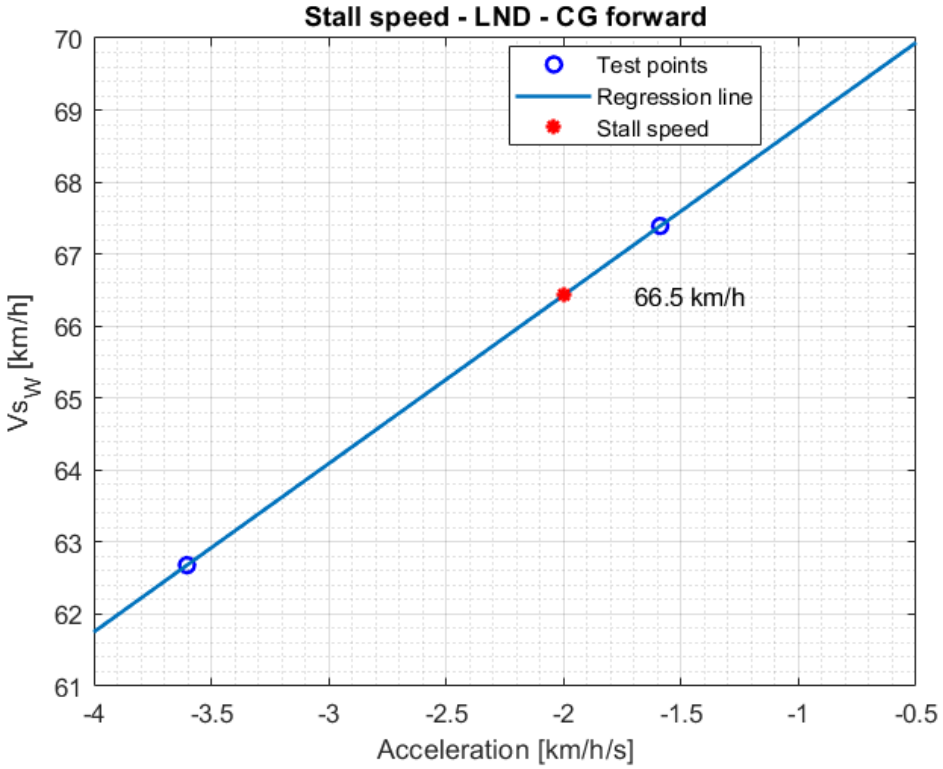


Figure 5.21: Stall speed - LND - CG forward

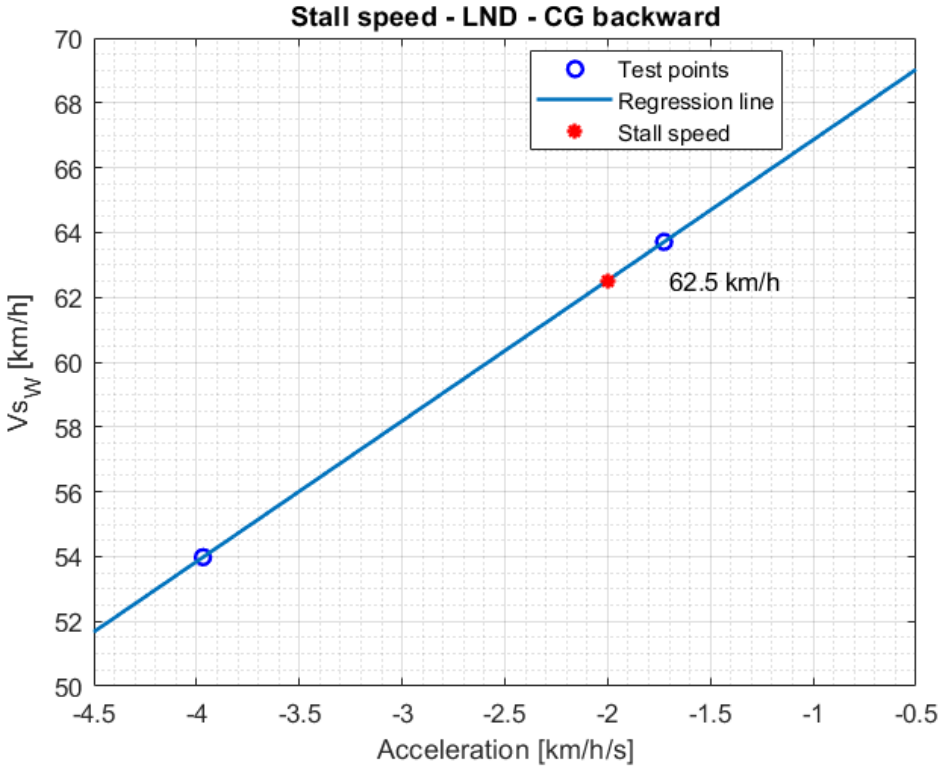


Figure 5.22: Stall speed - LND - CG backward

*Figure 5.20* shows the weight-reduced stall speed and AOA trends in LND configuration. It can be noticed that just before the stall, the A/C reaches almost 30 degrees of angle of attack. After this value the A/C stalls and rapidly increases its airspeed.

*Figure 5.21* is the most interesting figure in this chapter. In fact, as mentioned before, the maximum stall speed - with a deceleration of 2 km/h/s - imposed by the certification is 65 km/h. This speed value has to be tested with the CG in most forward position, which is the worst case for the stall speed. The weight-reduced stall speed showed in the graph is equal to 66.5 km/h. This value, even if is higher than 65 km/h, is considered acceptable by the German inspector. The reason is here explained: during the buildup of the A/C, the static pressure could be affected by a little change in the position or by the surrounding elements making its indication slightly different.

This important result permits the A/C to be certifiable also under the stall speed aspect.

*Figure 5.22* indicates the stall speed in the best condition, so with the center of gravity in the most backward position. As in the previous cases, the stall speed is lower than the one with CG in the most forward position.

### 5.2.5 Conclusions

The overall results are summarized in the following table. The indicated airspeed is the weight-reduced calibrated airspeed obtained with the CG in the forward position.

| Configuration | Stall speed [km/h] |
|---|---|
| CR | 73.2 |
| TO | 70 |
| LND | 66.5 |

Table 5.1: G70 stall speeds

In conclusion, the stall speeds have decreased significantly with respect to the former G70 (17). Its stall speeds were 85.4, 78.4, 77.3 km/h respectively in CR, TO and LND configuration. Thanks to the new flap modification the aircraft has decreased its stall speed in LND configuration from 77.3 km/h to 66.5 km/h. More than 10 km/h of difference. This improvement permits the A/C to meet the LTF-UL requirement about the stall speed. In fact, as mentioned before, even if the normative imposes a maximum stall speed of 65 km/h at the maximum weight of 472.5 kg, the result of 66.5 km/h has been considered valid from the German inspector.

This has been a very satisfying result since this success, together with the positive result of the anemometer calibration, have been reached for the first time for this model of aircraft.

## 5.3 Stall behavior

### 5.3.1 Introduction

The separate sections dedicated to this topic by LTF-UL, CS23 and CS-VLA underline its importance. Stall behavior means a qualitative and quantitative study of the reaction of the aircraft before, during and after the stall. According to sections 201 and 203 stall behavior has to be tested from idle throttle to MCP, both in level flight and in turning flight. This chapter presents only the tests performed with the throttle in idle and during a level flight. The other tests have been performed in a separate campaign by the German inspector.

### 5.3.2 Test objectives

The objective of this test is to assess the controllability of the aircraft and its attitude to regain the level flight without jeopardizing the safety of the operations. LTF-UL 201 states that:

- During the recovery, it must be possible to prevent more than 20° of bank, by the normal use of the controls.

- The loss of altitude from the beginning of stall until regaining level flight by applying normal procedures and the maximum pitch attitude below the horizon must be determined.

Besides, LTF-UL 207 prescribes an adequate stall warning. It can be either furnished through the inherent aerodynamic qualities – buffeting – of the airplane or by a device that clearly indicates the stall.

### 5.3.3 Test execution

Stall behavior tests have been performed together with the stall speed tests. So the way of execution is the same as in chapter 5.2.3.

### 5.3.4 Test results

In order to study this topic under each aspect, the results for each configuration will be presented together with a graph describing the typical trends of relevant parameters such as airspeed, altitude, pitch and roll angles.

In CR configuration the aircraft shows a clear roll brake with the right wing. This behavior can be noticed in the following figure.

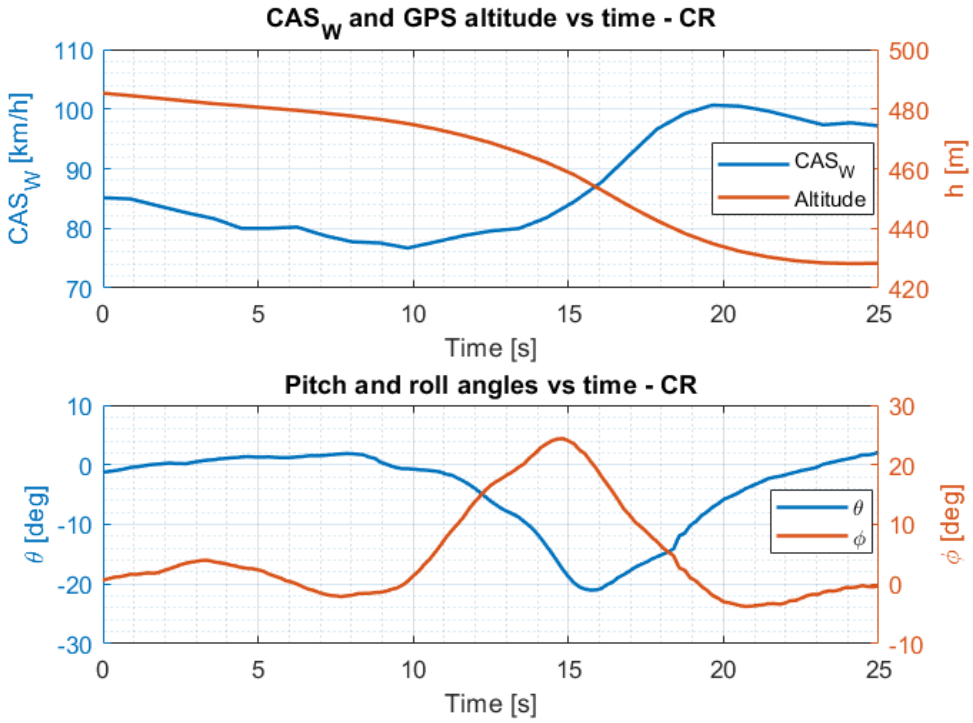


Figure 5.23: Stall behavior - CR

The roll angle Φ before the stall has a zero value, instead immediately after the stall, it reaches a value of 20°. However, in less than 5 seconds, the pilot is able to regain the level flight. The average loss of altitude in this configuration is about 72 meters, while the average pitch angle reached after the stall is about -27°.

In TO configuration, instead, the aircraft does not show a well-defined behavior. In fact in the eight stall tests performed in this configuration, four of them experienced only a pitch brake and the other four experienced a roll brake again with the right wing.

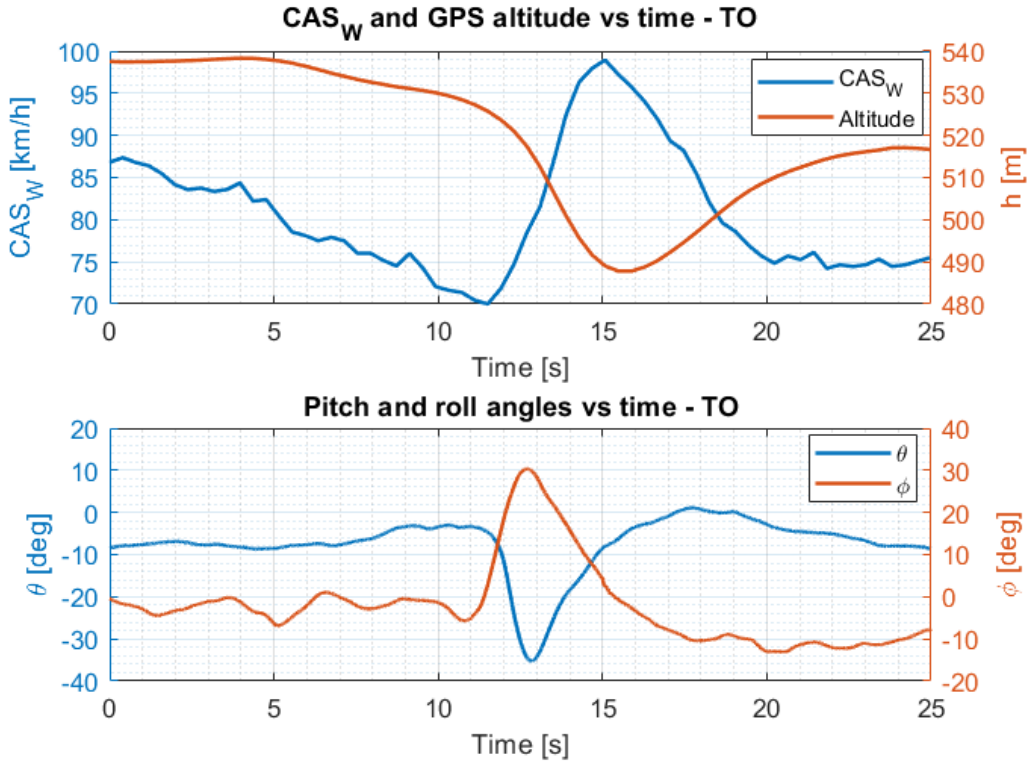


Figure 5.24: Stall behavior - TO - Roll brake

*Figure 5.24* clearly shows the roll brake experienced by the A/C.

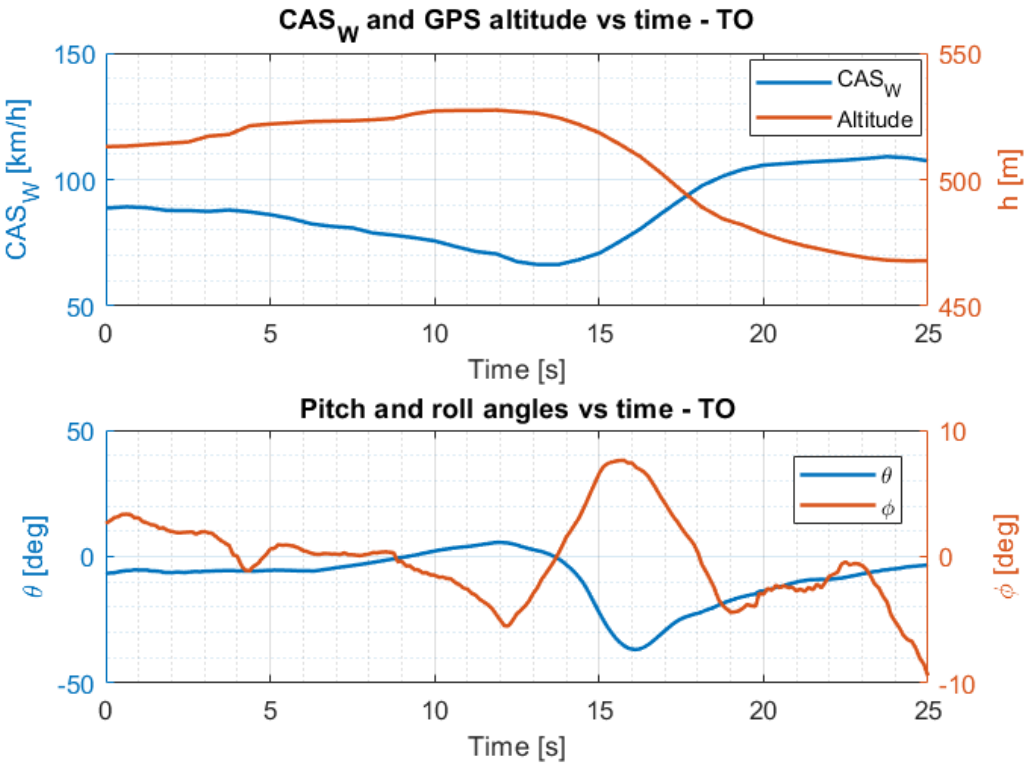


Figure 5.25: Stall behavior - TO - Pitch brake

*Figure 5.25* shows the pitch brake experienced by the A/C. It is evident, comparing the two figures, that in this case the roll angle Φ only oscillates of a few degrees while the pitch angle θ reaches a value of -40°.

Also in TO configuration the average loss of altitude is 65 meters, while the average pitch angle reached after the stall is -28°.

In LND configuration the aircraft experienced in all flights a pitch brake. Its behavior is presented in *Figure 5.26*.

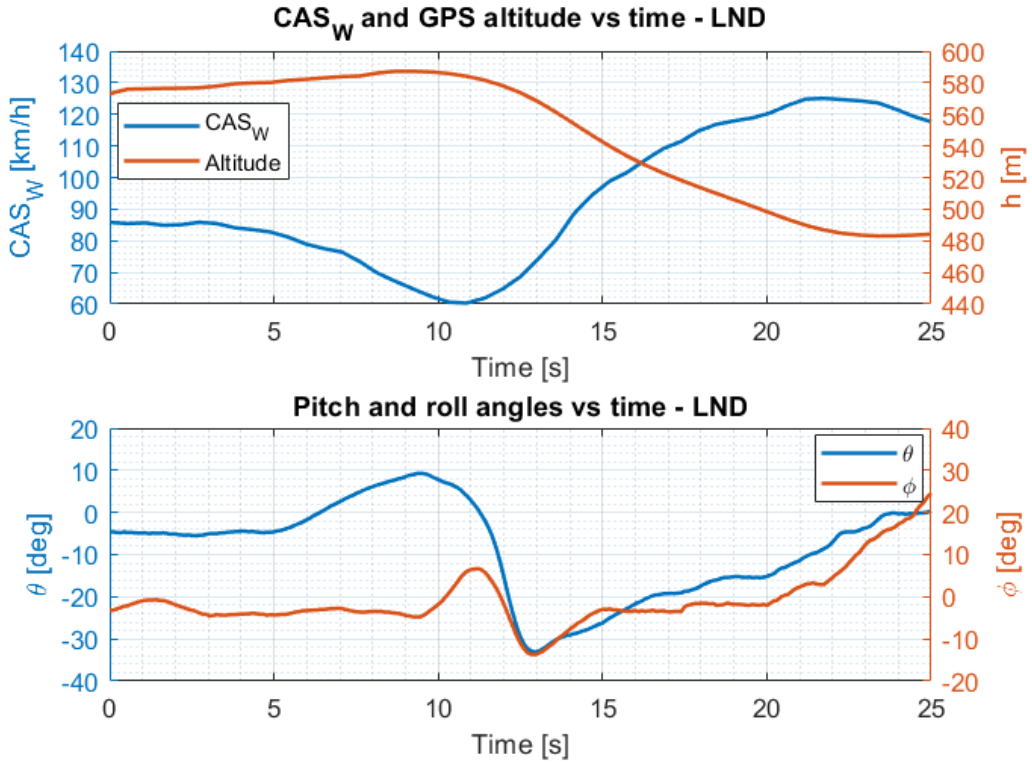


Figure 5.26: Stall behavior – LND

From this last figure it is evident the absence of a roll brake. Instead it is interesting to watch the pitch angle trend: it starts from a value of -5° and it reaches the value of +10° just before the stall. After this, the pitch angle θ reaches a value of -34°. So the pitch angle excursion has been of almost 45°.

The average pitch angle reached after the stall is -29° while the average loss of altitude is 64 meters.

It is important to underline that in all of these tests the pilot let the A/C to move freely at the stall, so he did not tried to limit the roll angle as imposed by the certification. This decision has been taken in order to deeply study the A/C behavior at the stall.

To demonstrate that it is possible to prevent more than 20° of bank during the stall, a dedicated stall test has been performed in flight 01.2605. In this test the pilot used the control stick to limit the A/C movements.

Test result is shown in *Figure 5.27*. The graph shows that if the pilot acts on the controls, he is able to prevent the roll angle to exceed the limit imposed by the normative.

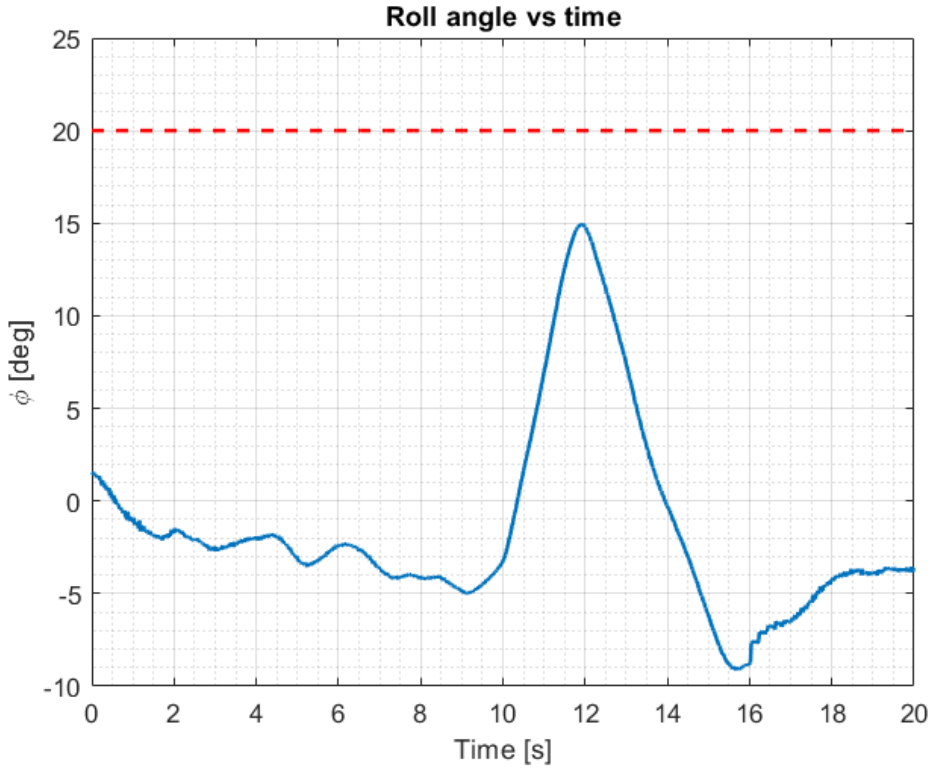


Figure 5.27: Roll angle during the recovery

### 5.3.5 Conclusions

The following table summarizes the results obtained.

| | Value |
|---|---|
| Average loss of altitude | 67 m |
| Average pitch angle | -28 deg |

Table 5.2: Stall behavior results

In conclusion, the aircraft behavior during the stall is satisfying, in fact the A/C results always able to regain the normal attitude without jeopardizing the safety of the operations. The roll limitations are satisfied as demonstrated before and the average loss of altitude is an acceptable value as well the average pitch angle reached after the stall.

# Chapter 6 – Performance testing

In this chapter, additional tests are considered concerning performance, and particularly Specific Excess Power (SEP), characterization. The so called Acceleration – Deceleration test technique was considered as an alternative to the traditional Sawtooth Climb technique. Acceleration – Deceleration tests, which are typically employed for high-performance aircraft, have been performed in order to investigate their suitability for SEP determination, in view of a characterization of the full flight envelope. Results and comparisons of the two methods are presented.

## 6.1 Acceleration – Deceleration test

### 6.1.1 Introduction

An aircraft in flight retains energy in two forms: kinetic energy and potential energy. Kinetic energy is related to the speed of the A/C, while potential energy is related to the altitude above the ground. The two types of energy can be exchanged with one another. When an A/C is in stabilized, level flight at a constant speed, the power has been adjusted by the pilot so that the thrust is exactly equal to the drag. If the pilot advances the throttle to obtain full power from the engine, the thrust will exceed the drag and the A/C will begin to accelerate. The difference in thrust between the thrust required for level flight and the maximum available from the engine is referred to as “excess thrust”. When the A/C finally reaches a speed where the maximum thrust from the engine just balances the drag, the “excess thrust” will be zero and the A/C will stabilize at its maximum speed.

It must be noticed that this “excess thrust” can be used either to accelerate the A/C to a higher speed – increase the kinetic energy – or to enter a climb at a constant speed – increase the potential energy – or some combination of the two.

There are energy exchange equations which can be used to relate the rate of change of speed to the rate of change of altitude, these equations will be presented later. In this way, level flight accelerations at maximum power can be used to

measure the “excess thrust” over the entire speed range of the A/C at one altitude. This “excess thrust” can then be used to calculate the maximum rate of climb capability for the A/C.

### 6.1.2 Test objectives

The test objective is to determine the acceleration capability – excess thrust – at a particular altitude over the entire speed range of the G70. Moreover, this permits to indirectly determine the rate of climb capability at the selected altitude over the entire speed range of the A/C.

### 6.1.3 Test execution

The procedure which has been followed for this test is the one described in a NASA document (5).

The procedure is the following:

1. The pilot has to trim the A/C at the desired altitude at a speed that lies in the center of the speed range of the A/C. For the G70 the speed is 130 km/h.
2. The pilot uses the trim devices to allow the A/C to continue in stable, level flight, but with the pilot’s hands and feet off of the controls.
3. The pilot reduces the power to idle and decelerates to the minimum desired speed, usually a few km/h above the stall (for the G70 100 km/h), while holding the A/C at exactly the same altitude by using only the pitch control.
4. The pilot moves the throttle, smoothly but quickly, to full power and allow the A/C to accelerate while maintaining the same altitude again using only the pitch control.
5. When the maximum speed has been reached the pilot reduces the power to idle and decelerate back to the starting trim speed, continuing to stay at the same altitude.

The test is considered successful if meets the following requirements:

1. Maximum altitude variation: ± 100 ft
2. Smooth power transition between idle and max.

### 6.1.4 Data reduction

Since the inertial measurement unit is mounted as shown in the following figure and we want to obtain the acceleration on the trajectory line of the A/C, one operation has to be done (pitch correction).

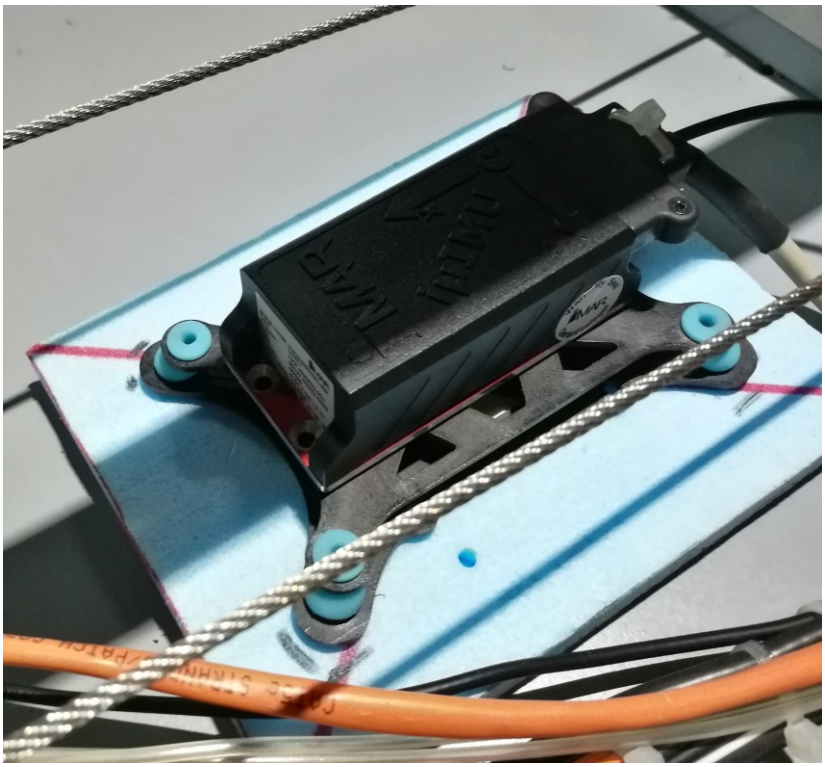

Figure 6.1: IMU mounted on the A/C

It can be noticed that the X-axis points to the back of the A/C, while the Y-axis to the right wing and the Z-axis points up, perpendicular to the aircraft.

The so-called pitch correction is the following:

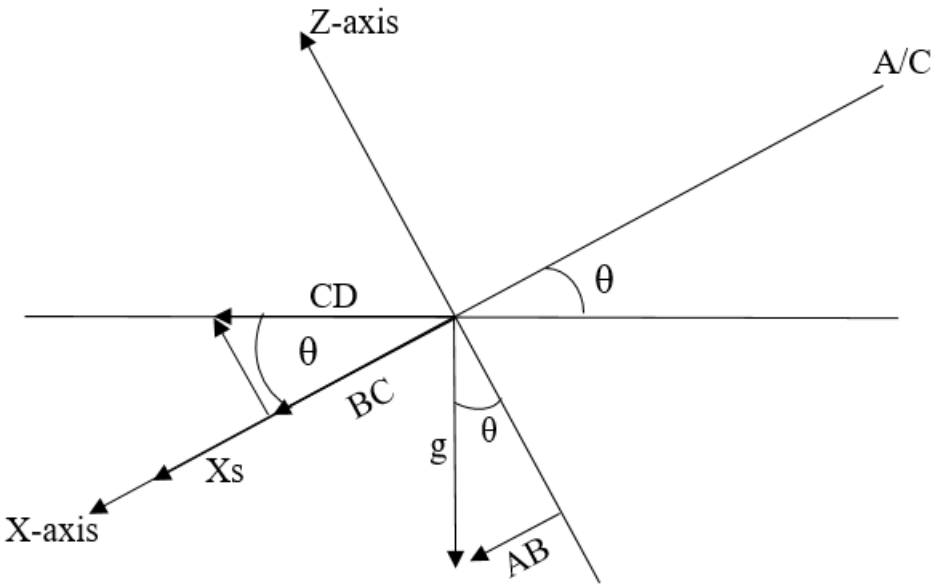


Figure 6.2: Pitch correction

The IMU on its X-axis measures Xs and

$$Xs = AB + BC$$

Our desired parameter is CD and in order to obtain it, first we have to remove the AB contribute and, after this, to obtain the projection of BC on the trajectory axis. So:

$$CD = \frac{Xs - g\sin\theta}{\cos\theta}$$

The sideslip correction has not been considered since the contribution of this correction is minimal. From this point the acceleration on the trajectory line will be called $a_X$, while the perpendicular to the trajectory $a_Z$.

The following figure shows the complete time history of TAS, altitude, pitch angle, roll angle, $a_X$ and $a_Z$ during the flight test 01.2605.

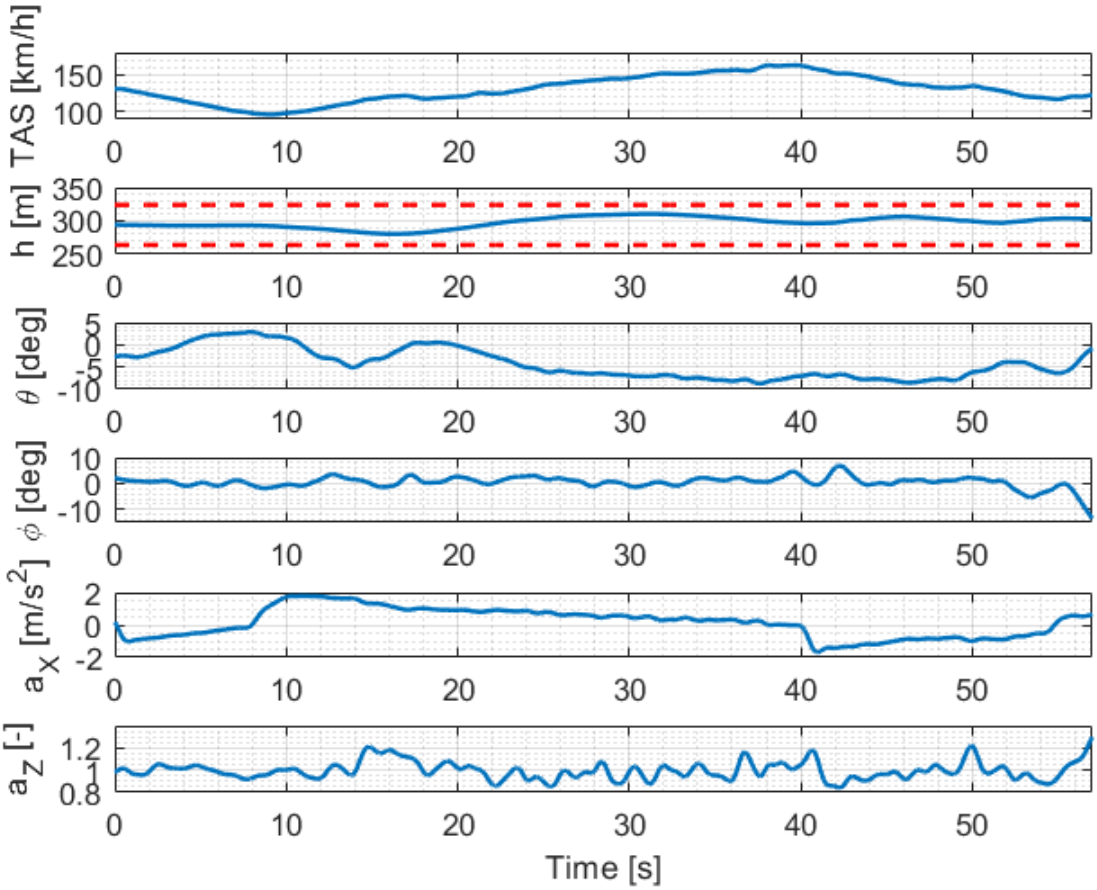


Figure 6.3: Complete time history

From the altitude plot it is clearly showed that the pilot has been able to keep the A/C between the two red lines that rapresent the maximum altitude tolerances. Instead from the TAS plot it can be noticed that the speed has a non-linear behavior from second 15 to second 25. This trend suggests the presence of a gust during the test. This fact is confirmed also observing the $a_Z$ plot: between these seconds the normal acceleration oscillates in a different way with respect to the remaining acceleration phase.

In particular, the gust hit the A/C from behind. In fact the TAS decreases while the GS increases; this is shown in *Figure 6.4*.

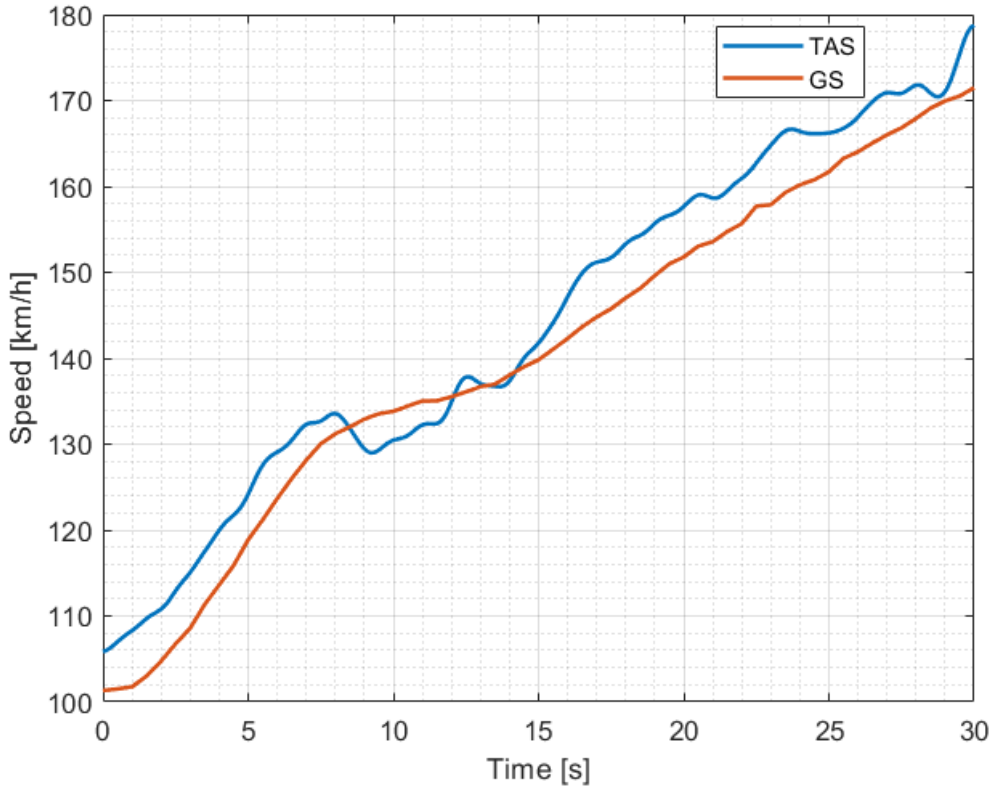


Figure 6.4: TAS and GS - Acceleration phase

Because of this non-linearity during the acceleration phase, a mathematical process has been done in order to reduce gust and wind effects. In particular, the mean square error method has been used. The speed lines – TAS and GS – have been cut and divided into two parts excluding the gust segment. This two parts have been called “Superior segment” and “Inferior segment”. The mean square error method has been applied to these two parts and its goal is to find the value that minimize the difference between the two speeds. In this way we can get rid of wind and gust effects.

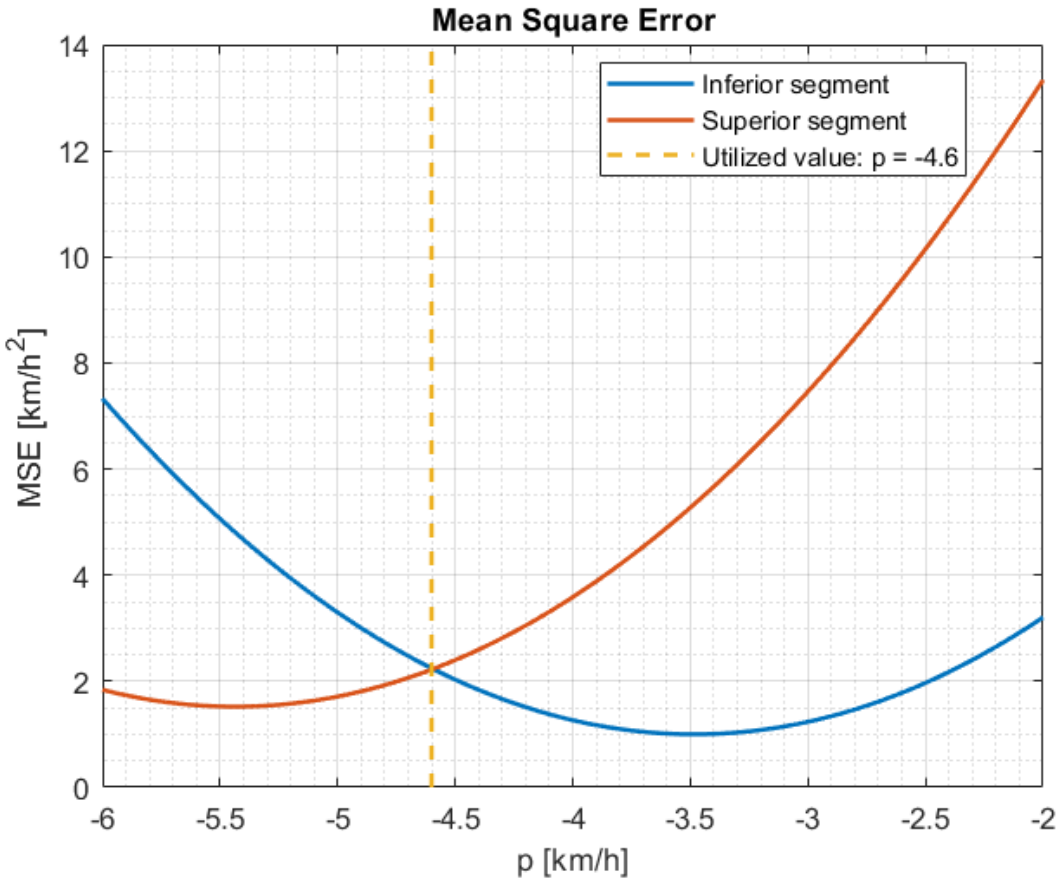


Figure 6.5: Mean square error

*Figure 6.5* shows the error trend when varying the parameter p. In order to minimize both errors the chosen value is p = - 4.6 km/h.

After this, the following step is to substitute the GS part characterized by the gust with a straight line. The substituted part starts from 122 km/h and finishes at 145 km/h. Done this, the value of p has to be subtracted to the new GS. In this way we obtain the speed line – called "TAS modified" – that we will use to calculate the "excess thrust".

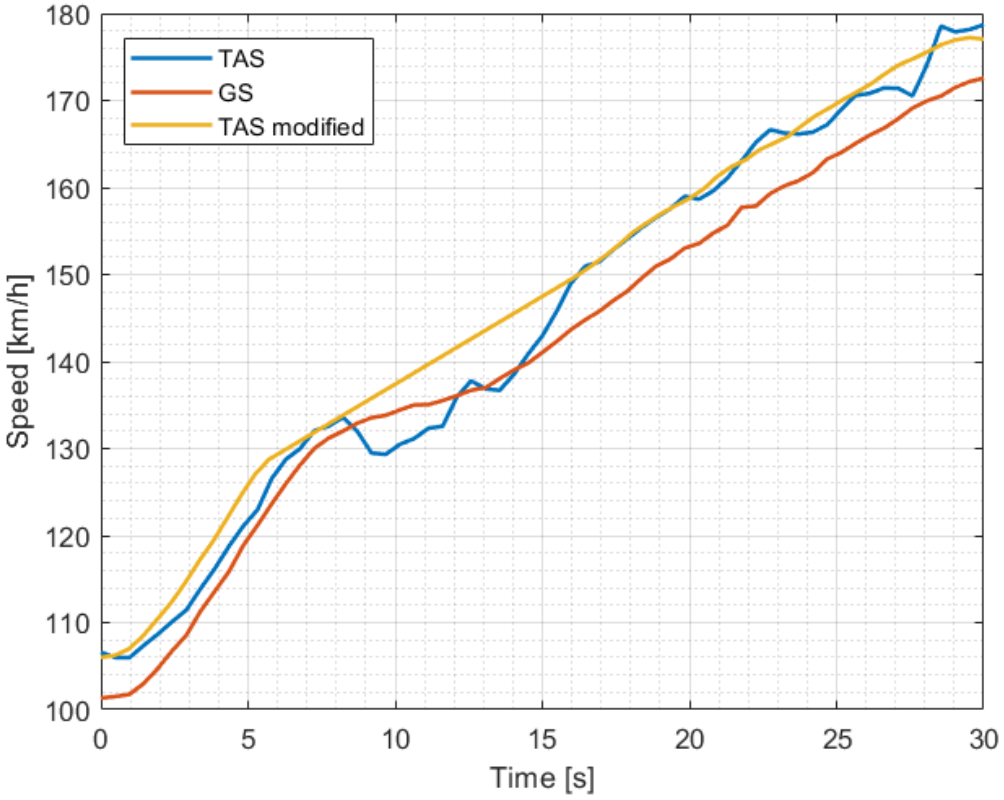


Figure 6.6: TAS, GS and TAS modified – Acceleration phase

*Figure 6.6* shows the initial TAS and GS and the final TAS modified obtained with the above said method. It can be noticed that its trend approximates the TAS in a good way and the gust effect has been eliminated.

Moreover, in order to get a result comparable with other test results obtained in different ambient conditions, we have to consider both the temperature effect on the engine performances and the aircraft weight.

In order to evaluate the power supplied variation due to the temperature variation we have to introduce the following parameter:

$$\frac{\Delta R}{C1} = \frac{33000 \times BHP_T}{W_T}\left[\sqrt{\theta} - \frac{1}{\sqrt{\theta}}\right]\eta_{prop}$$

Finally we obtain the corrected rate of climb with this final equation that take in consideration also the weight variation with respect to the standard weight:

$$ROC_C = \left(ROC \times \sqrt{\theta} + \frac{\Delta R}{C1}\right)\left(\frac{W_T}{W_S}\right)$$

### 6.1.5 Test results

The energy exchange relationship mentioned in the introduction is defined by the following mathematical expression:

$$Fne = \frac{W}{g}\left(\frac{dV}{dt}\right) + \frac{W}{V}\left(\frac{dh}{dt}\right)$$

where:

$Fne$ = excess thrust;

W = weight of the airplane;

g = acceleration due to gravity;

V = velocity;

$\left(\frac{dV}{dt}\right)$ = rate of change of velocity;

$\left(\frac{dh}{dt}\right)$ = rate of change of altitude.

During a level flight acceleration we have forced the second term in the equation to be zero by flying at constant altitude, so the rate of climb is null. The excess thrust can be computed by measuring the acceleration and weight. So we obtain:

$$Fne = \left(\frac{W}{g}\right) \times \left(\frac{dV}{dt}\right)$$

The equivalent rate of climb can be computed by forcing the first term to zero by assuming a climb at constant speed, so that the acceleration is null.

The equation obtained is:

$$Fne = \left(\frac{W}{V}\right) \times \left(\frac{dh}{dt}\right)$$

or, rearranging:

$$\left(\frac{dh}{dt}\right) = Fne \div \left(\frac{W}{V}\right)$$

This calculation produces a curve that relates the rate of climb with respect to the airspeed.

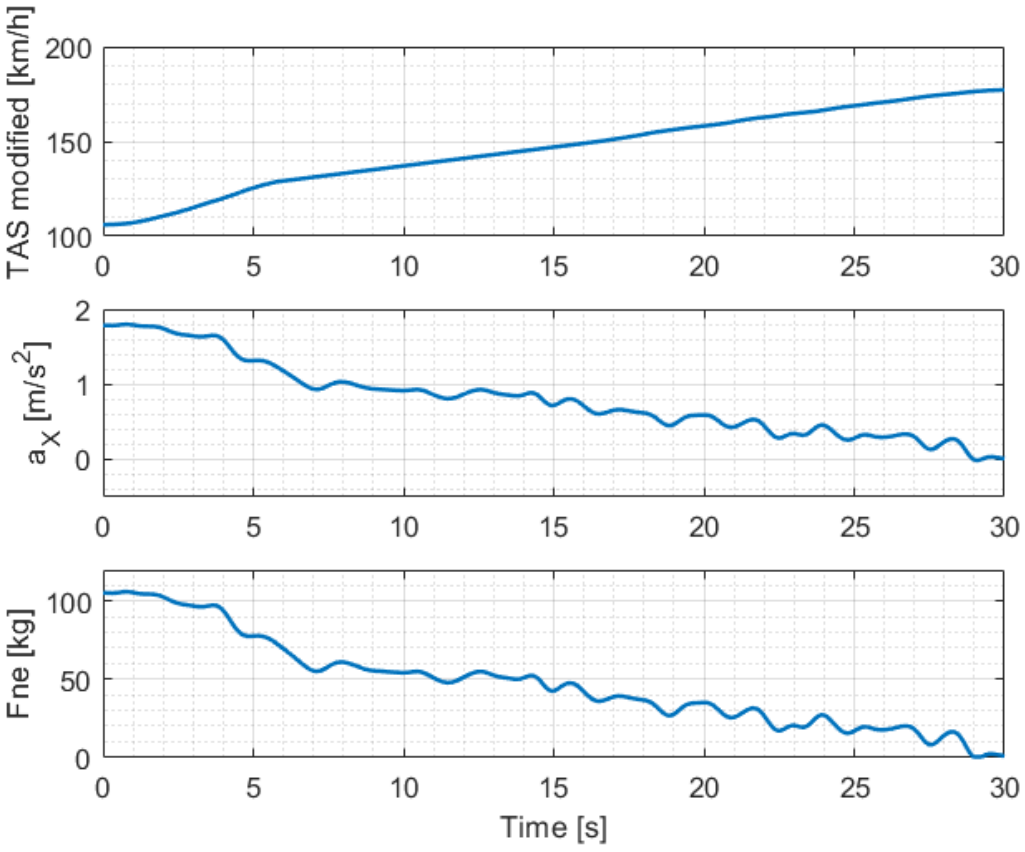


Figure 6.7: TAS, acceleration and excess thrust - Acceleration phase

*Figure 6.7* shows the obtained results: the TAS modified is the one obtained in the previous chapter, the acceleration is the one on the trajectory line while $Fne$ is

the excess thrust. It can be noticed that, as perceivable, its maximum is at the beginning of the acceleration, when the value of the acceleration reaches its maximum. Excess thrust and acceleration trends are the same since the former strictly depends on the latter. In fact for this test the weight has been considered a constant value due to the test brevity.

Applying the last equation above mentioned, we obtain the following plot. It refers to a standard weight of 472.5 kg.

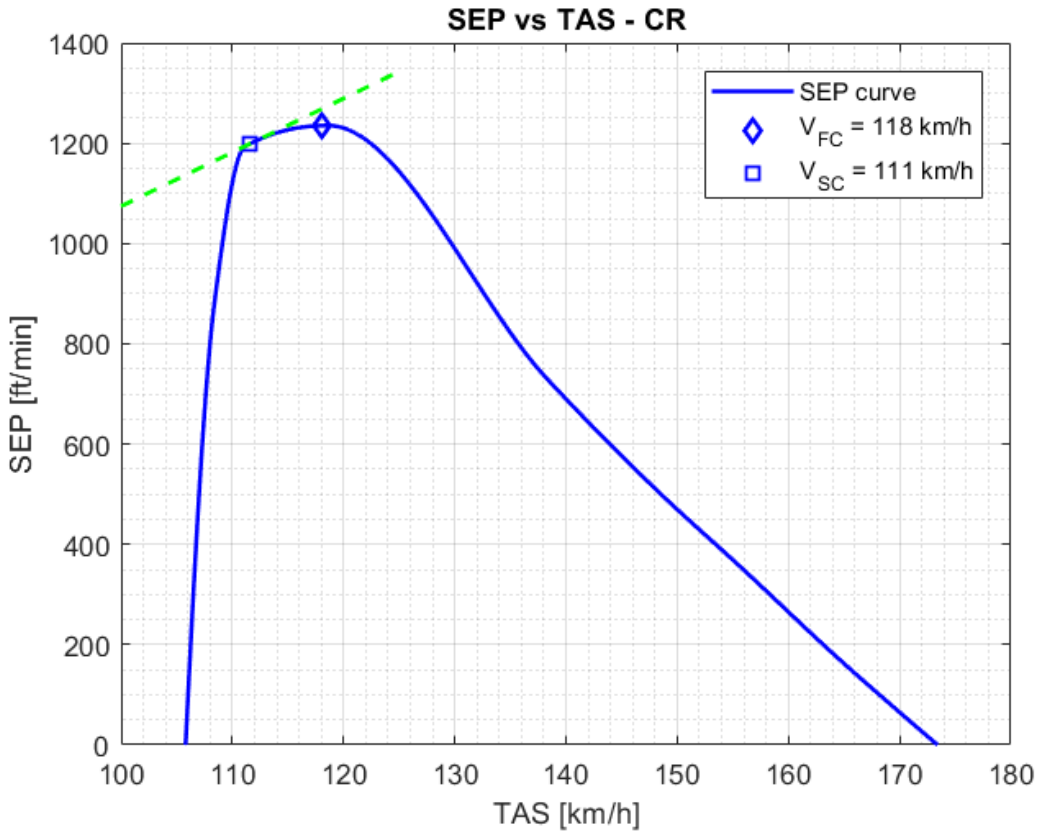


Figure 6.8: SEP - CR - 1000 ft - Acceleration deceleration test

The SEP curve indicates the $V_{FC}$ at 118 km/h with a SEP value of about 1235 ft/min. Instead the $V_{SC}$ is identified at 111 km/h with a SEP value of about 1200 ft/min. The following table summarizes the results.

| Flap conf. | $V_{FC}$ [km/h] | $V_{SC}$ [km/h] | $MAX_{ROC}$ [ft/min] |
|---|---|---|---|
| CR | 118 | 111 | 1235 |

Table 6.1: Climb performances - CR - 1000 ft - Acc Dec

## 6.2 Sawtooth climb test

### 6.2.1 Introduction

This test has been performed by the Flight testing course students. The author has taken their raw data about this test and post-processed them in order to compare the result of this test with the one of the Acceleration – Deceleration test. Since the former test has been executed only in CR configuration the result for the only CR sawtooth climb test will be shown. A brief theory of this test is described in Appendix B – Climb performance theory.

### 6.2.2 Test objectives

This test provides speed of fastest and steepest climb for the aircraft. These results will be compared with the ones of the Acceleration – Deceleration test.

### 6.2.3 Test execution

The sawtooth climb test is the normally performed test in order to obtain the aircraft climb performances. The test consists in a series of climb segments, flown through the same altitude gap with full throttle. Every climb has flown with a different speed in order to sweep a sufficiently broad range of velocities to provide a good second order approximation. In particular three different speeds have been utilized together with a maximum speed trim shot. This last point is necessary to provide the closing point of the curve since its rate of climb is null.

The following test procedure is obtained from CS23-FTG (4):

1. Set the flap in CR configuration;
2. Trim the A/C sufficiently below the entry altitude;
3. Full throttle;
4. Start climbing and time the climb, the pilot has to maintain the same airspeed throughout the whole climb;

5. When reached the upper altitude, set power as necessary and descend in order to repeat the climb along the same altitude range but with a different airspeed.

Dividing the altitude gap for the time to climb we obtain the raw rate of climb. At this point a normalization is needed. Since LTF-UL prescribes only a correction for the Atmosphere Sea Level, also the procedure described in (7) has been followed.

### 6.2.4 Data reduction

The following step have been followed in order to get a correct data reduction:

1. Calculate the raw ROC from the pressure altitude slope:

$$\left(\frac{\Delta h}{\Delta t}\right)_m$$

2. Normalize with respect to the standard temperature, by multiplying the test temperature $\Theta_T$ versus the standard temperature at the height of the test $\Theta_S$:

$$\left(\frac{\Delta h}{\Delta t}\right)_t = \left(\frac{\Theta_T}{\Theta_S}\right)\left(\frac{\Delta h}{\Delta t}\right)_m$$

3. Correct for the actual power $P_b$, temperature deviation, test weight $W_T$ and propeller efficiency:

$$\Delta\left(\frac{\Delta h}{\Delta t}\right)_P = \frac{\eta_p P_b}{W_T}\left(1 - \sqrt{\frac{\Theta_S}{\Theta_T}}\right)$$

4. Correct for TAS variation with altitude:

$$\Delta\left(\frac{\Delta h}{\Delta t}\right)_{AF} = \frac{V}{g}\left(\frac{dTAS}{dh}\right)\left(\frac{\Delta h}{\Delta t}\right)_{t}$$

5. Correct all the previous contributions with respect to standard weight $W_S$:

$$\left(\Sigma\frac{\Delta h}{\Delta t}\right)\frac{W_T}{W_S}$$

6. Correct for induced drag due to a non-standard weight:

$$\Delta\left(\frac{\Delta h}{\Delta t}\right)_{ind} = \frac{2}{\pi\lambda e\sigma\rho_0 V_{TAS} S}\left[\frac{W_T^2 - W_S^2}{W_S}\right]$$

The final equation is:

$$\left(\frac{\Delta h}{\Delta t}\right)_{std} = \left[\left(\frac{\Delta h}{\Delta t}\right)_{t} + \Delta\left(\frac{\Delta h}{\Delta t}\right)_{P} + \Delta\left(\frac{\Delta h}{\Delta t}\right)_{AF}\right]\frac{W_T}{W_S} + \Delta\left(\frac{\Delta h}{\Delta t}\right)_{ind}$$

### 6.2.5 Test results

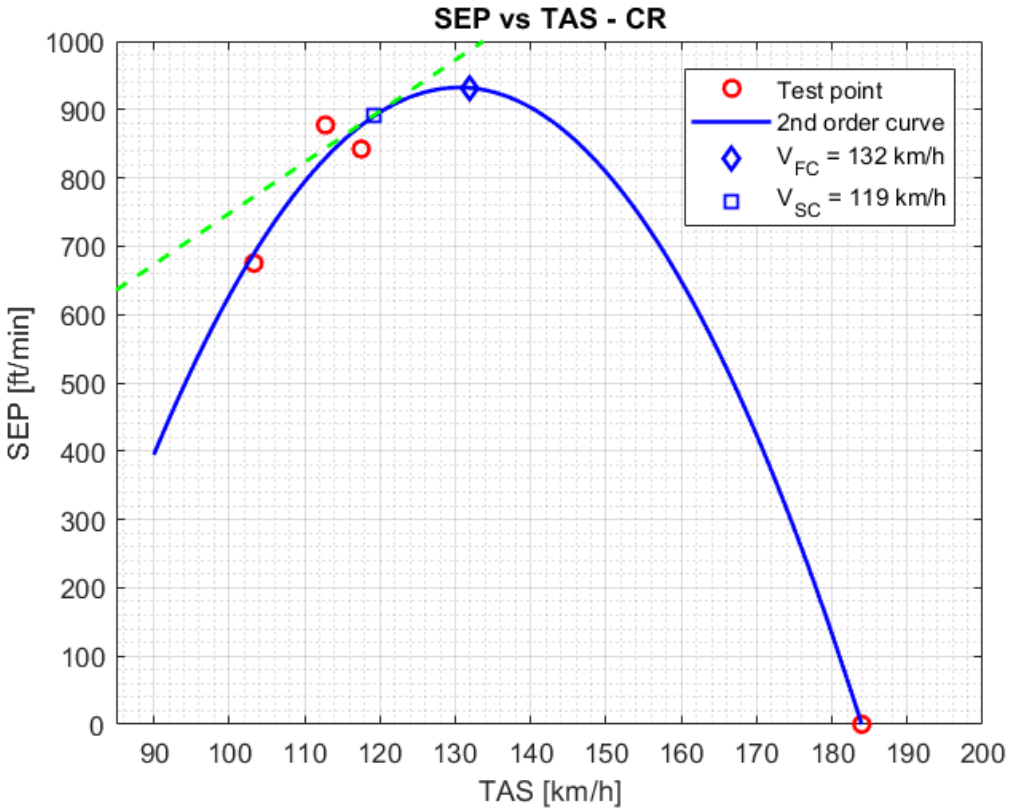


Figure 6.9: SEP - CR - 1000 ft - Sawtooth test

*Figure 6.9* shows the result obtained from the sawtooth test. The red dots are the test point flown and the SEP curve is obtained with a second order curve. The SEP curve indicates the $V_{FC}$ at 132 km/h with a SEP value of about 930 ft/min. Instead the $V_{SC}$ is identified at 119 km/h with a SEP value of about 890 ft/min. The following table summarizes the results.

| Flap conf. | $V_{FC}$ [km/h] | $V_{SC}$ [km/h] | $MAX_{ROC}$ [ft/min] |
|---|---|---|---|
| CR | 132 | 119 | 930 |

Table 6.2: Climb performances - CR - 1000 ft - Sawtooth climb

## 6.3 Comparison between the two test methods and conclusions

First of all, it must be underlined that the Acceleration – Deceleration test is much less time consuming with respect to the Sawtooth climb test. In fact the latter requires about five minutes to gather the test points data plus the time required to regain the correct test altitude between each climb. The former, instead, takes about one minute to gather all necessary test data. So it lasts at least five time less than the Sawtooth climb test. This fact could permit to save considerable time during the campaign.

After this aspect about time, it is necessary to compare the results of the two test.

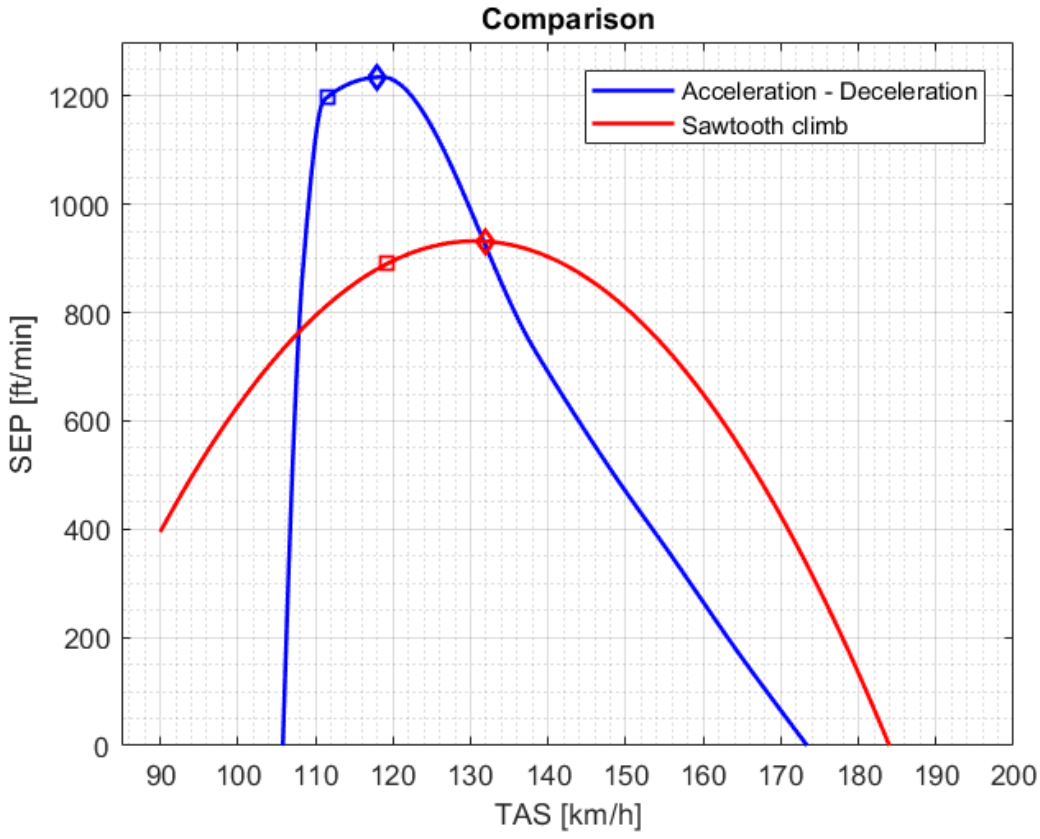


Figure 6.10: Acc-Dec and Sawtooth climb comparison - CR - 1000 ft

As clear from *Figure 6.10* there is a big difference between the two results. In particular, the Acc-Dec SEP reaches its maximum more than 10 km/h earlier than the Sawtooth SEP maximum. Besides the highest SEP value in the first test is almost 300 ft/min major than the one of the second test.

Another big difference is the gap between the two curves after the speed of 130 km/h: this is probably due to the fact that in the Sawtooth climb test the curve is approximated with a second order curve that is originated from the test points. The problem of this approximation is that the test points are present only in the first speed range, at low speeds. So there are no test points over the speed of 115 km/h. Because of this the reliability of the curve after that speed is questionable.

Instead the strength of the Acc-Dec test is that it permits to plot a complete curve without important approximations because the test itself allows to gather data throughout the entire speed range of the aircraft. This is an important thing since, as we have just seen, the resulting curve better describes the real performances of the aircraft.

In fact, the Pilot Operating Handbook (6) declares a maximum ROC at 1000 ft of 1300 ft/min at the speed of 110 km/h (CAS). Besides the declared steepest climb speed is equal to 100 km/h (CAS) with a ROC of almost 1270 ft/min. It must be underlined that these values are indicatives, in fact they have been obtained after many flights performed by the manufacturer.

The results of the two tests and the POH data are here reported:

| | $V_{FC}$ [km/h] | $V_{SC}$ [km/h] | $MAX_{ROC}$ [ft/min] |
|---|---|---|---|
| Acc - Dec | 118 | 111 | 1235 |
| Sawtooth climb | 132 | 119 | 930 |
| POH | 110 | 100 | 1300 |

Table 6.3: Performances comparison - CR configuration - 1000 ft

The table clearly shows the big discrepancy between Sawtooth climb and POH; there are more about 20 km/h of difference between the two results. Instead the difference sensibly decreases comparing the POH data with the Acc – Dec results: the difference is about 10 km/h. Thanks to this comparison table the goodness of the Acc – Dec test is shown.

In conclusion, the Acceleration – Deceleration test is a good substitute of the Sawtooth climb test. The first reason is the major accuracy of the result throughout the entire flight envelope; the second reason is the fact that is timesaving.

The only negative aspect of this test is that is very susceptible to the external factors, such as wind and gust effects. The presence of these factors negatively affect the result. The suggestion of the author is to perform this test in the early morning or in the late afternoon in order to limit the presence of the above-mentioned external factors.

# Chapter 7 – Conclusions

At the end of this thesis work, it is possible to affirm that all goals have been achieved. In fact, the third model of G70 accomplishes all regulation requirements imposed by German LTF-UL certification standard.

In particular, this new model satisfies the requirements concerning anemometer calibration, which was not the case for the previous versions. This permits the pilot to have a reliable airspeed lecture throughout the entire speed range in all flap configurations. It must be underlined that the previous version of the aircraft could comply with the certification requirements only placing the static pressure probe inside the cabin, which is not a certifiable situation.

Moreover, the second model of G70 had a stall seed of nearly 75 km/h in LND configuration. This new model, thanks to the introduction of a plastic foil that closes the gap between wing and flap, has a stall speed of 66 km/h. Thanks to this result, the aircraft satisfies also the stall speed requirement imposed by the norms. Besides, the aircraft does not show any dangerous behavior at the stall and after it, and it remains within the limitations of the LTF-UL at all times, fully satisfying also stall behavior requirements.

These results, together with the tests executed by the German inspector, permitted the aircraft to receive the certification at the end of this test campaign. In fact, a LTF-UL type certificate was granted to the NG G70 in April, 2018, after more than two years work by Ing. Nando Groppo Srl with the support of DAER-PoliMI.

The Acceleration – Deceleration tests, performed at the end of the campaign, have given very good results and have shown their suitability in aircraft performances studies. In particular, thanks to this test it is possible to determine the Specific Excess Power performance of the aircraft throughout the entire speed range, at a given altitude. This is an important quality of this test when compared to the Sawtooth Climbs test. In fact, the latter permits to create a second order curve that well approximates the performances of the aircraft at low speeds, near the test points, but accuracy may be lost at higher speeds. In conclusion, the Acceleration –

Deceleration test can be considered a valid substitute of the Sawtooth Climbs test, paying attention to insure adequate test conditions.

The author wants to underline the importance that has to be given to test planning and to flight card preparation. In fact, during a test flight, one should minimize the occurrence of problems that were not taken into account during planning. In order to get a refined planning capability, it is necessary to accumulate substantial experience and to accurately foresee what has to be done during the flight. In fact, it may be also difficult to manually record many parameters during the flight, so the FTE has to properly set up priorities in data gathering.

Moreover, the pilot has to pay attention on the flight management during the entire mission, in order to keep the aircraft as close as possible to the conditions to be investigated. If the aircraft is brought too far from the desired test condition, the test has to be repeated, losing time and money.

A final consideration may be done about test repeatability. With an aircraft featuring light weight and relatively modest performance, it is difficult to get always the same test results when tests are performed in different days and hours of the day. In fact, may elements of the flight behavior of this type of aircraft are strongly affected by the local atmospheric conditions. In order to limit this impact, it has been necessary to perform the tests in the early hours of the day or in the late afternoon.

# Appendix A

# Air data calibration

**Anemometer calibration – Flight 01.1302**

The first air data calibration took place in the first flight. The configuration was the one with only the Pitot tube mounted under the left wing as shown in *Figure A.0.1*.

Figure A.0.1: Pitot tube, 1st attempt

The results were completely unsatisfactory as can be clearly seen in the following figures.

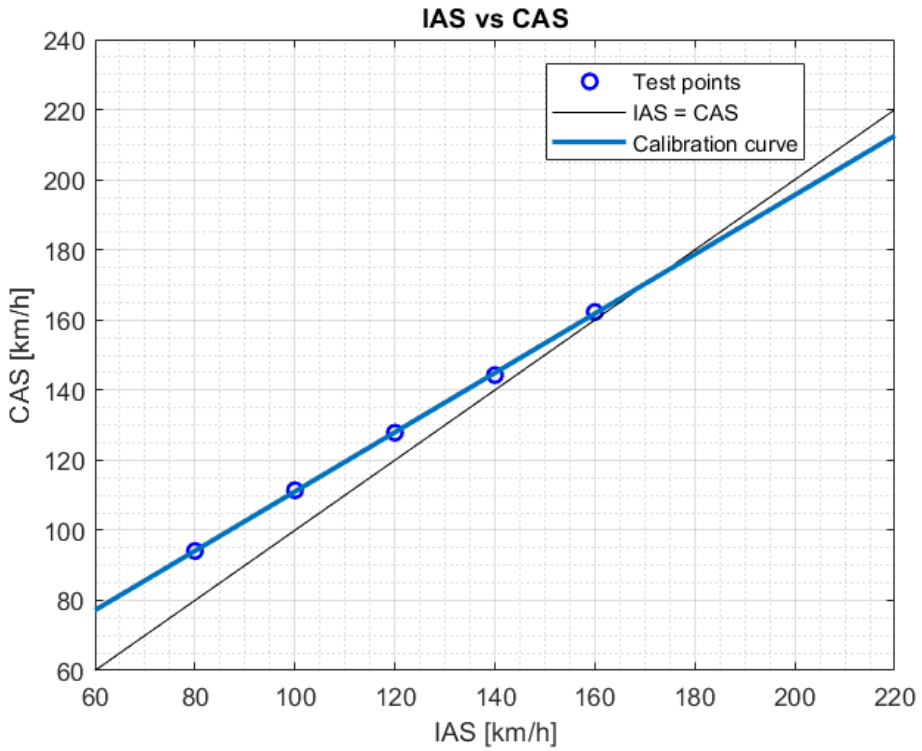


Figure A.0.2: IAS vs CAS - CR configuration - flight 01.1302

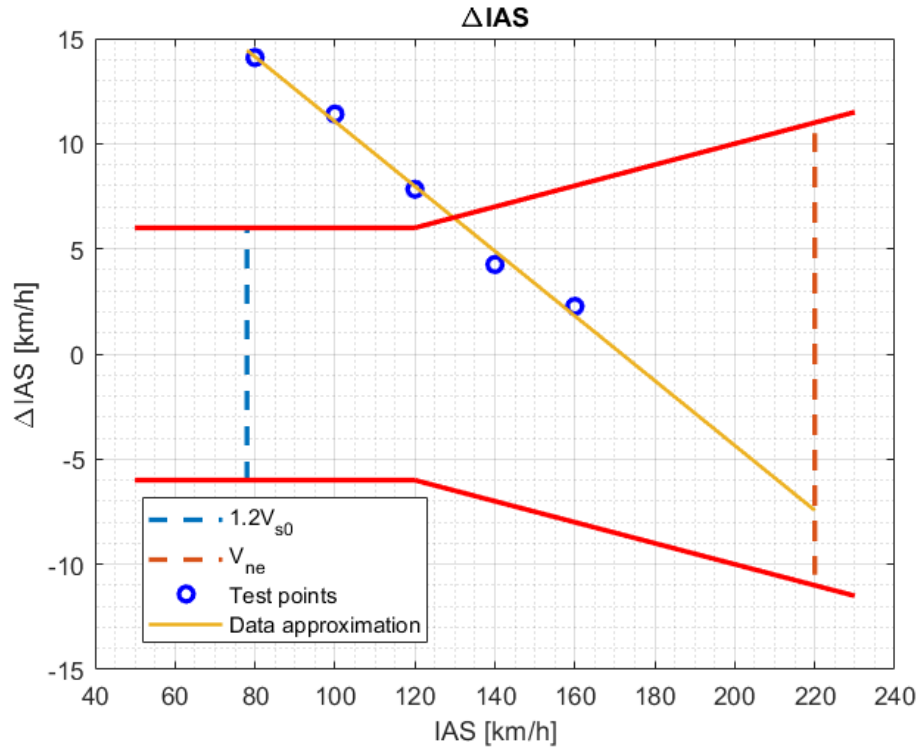


Figure A.0.3: IAS error - CR configuration - flight 01.1302

In particular at low speeds the error is quite big, almost 15 km/h.

Because of the high error at low speeds, the author and the TP thought that the solution was to increase the stagnation around the static probe in order to increase the static pressure and so decrease the dynamic one. This reasoning has been done thinking that the error of the total pressure probe was null.

**Anemometer calibration – Flight 01.1502**

In order to increase the static pressure two O-rings have been added behind the static port and one in front of it, as shown in *Figure A.0.4*.

Figure A.0.4: Pitot tube - 2nd attempt

As forecast, the new configuration increased the static pressure, however again the result was unacceptable.

In *Figure A.0.5*, it can be noticed that the slope of the calibration curve is unchanged with respect to the one showed in *Figure A.0.2*: only the offset has changed.

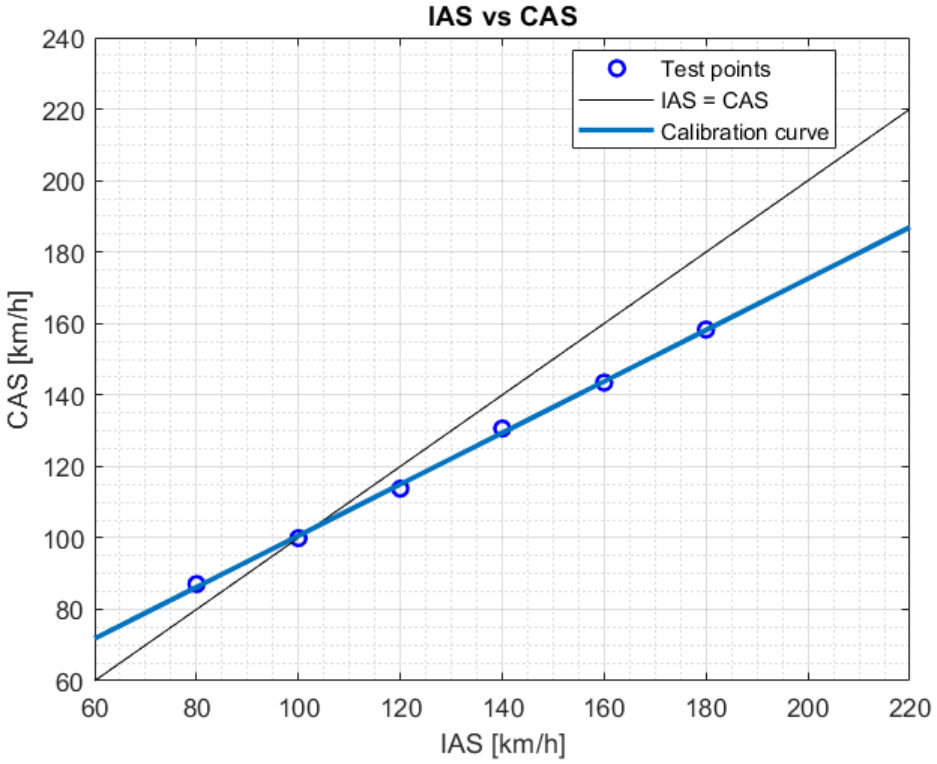


Figure A.0.5: IAS vs CAS - CR configuration - flight 01.1502

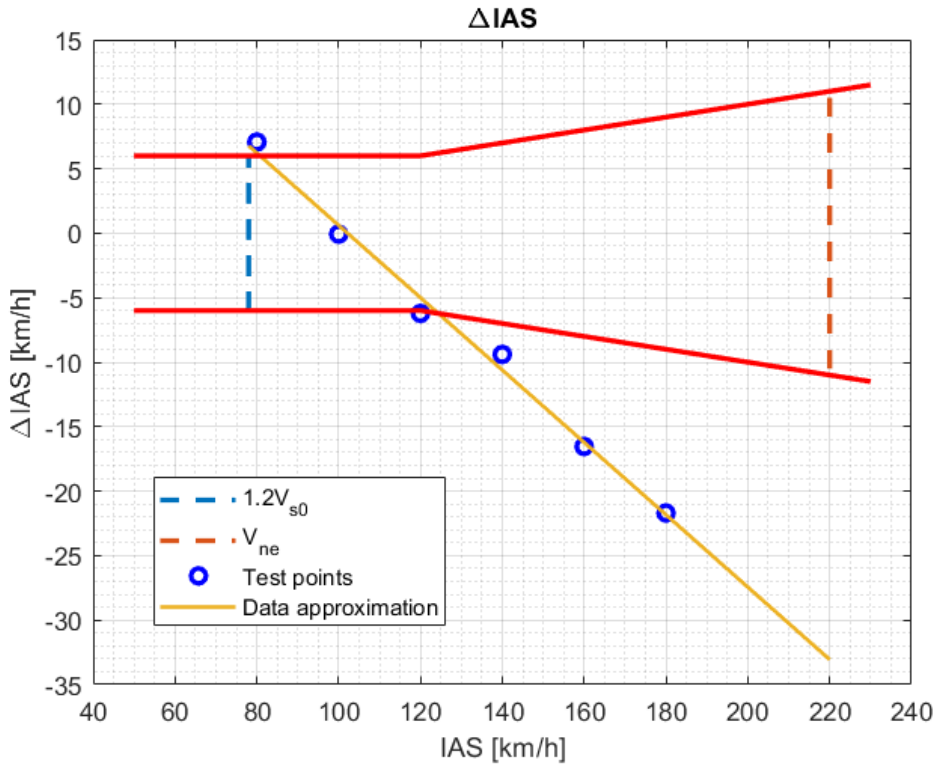


Figure A.0.6: IAS error - CR configuration - flight 01.1502

In this case, the error at low speeds decreased but, as a consequence, the error at high speeds increased too much. Over the speed of 120 km/h the error is considered unacceptable according to the certification.

**Anemometer calibration – Flight 02.1502**

The third attempt has been performed adding only one O-ring in front of the static port. The results are presented in the following figures:

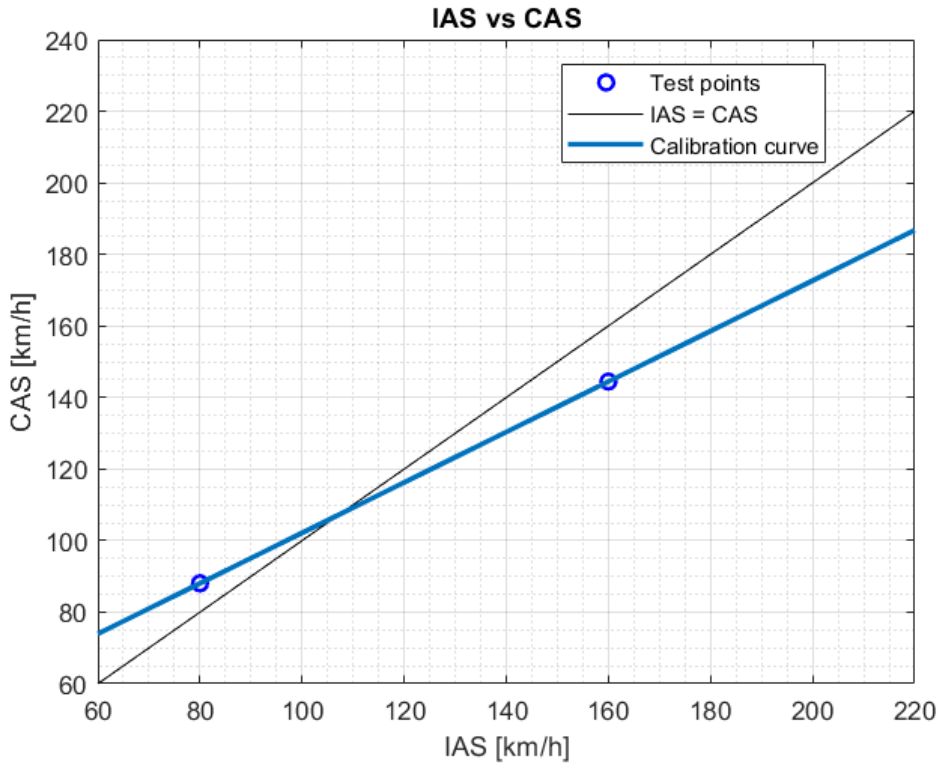


Figure A.0.7: IAS vs CAS - CR configuration - flight 02.1502

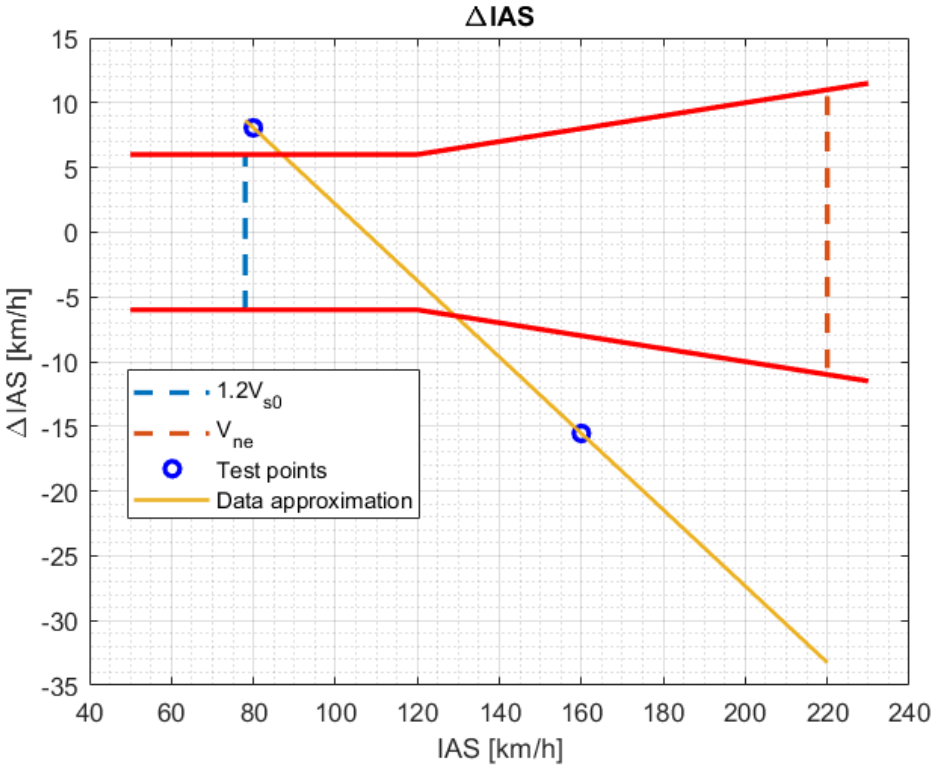


Figure A.0.8: IAS error - CR configuration - flight 02.1502

This time only two test points have been performed in order to decrease the flight duration, it must be underlined that this decision does not void the test.

It can be noticed that even this attempt has to be considered unacceptable. It is useful to underline that there is no an important deviation from this attempt and the previous one: this fact suggests that the presence of the O-rings behind the static port does not have any particular relevance.

**Anemometer calibration – Flight 03.1502**

In order to confirm the above said fact, the flight 03.1502 has been performed with only one O-ring behind the static probe, as shown in *Figure A.0.9*.

Figure A.0.9: Pitot tube - 4th attempt

The results are not presented since only one test point was performed since the error was immediately noticed to be unacceptable: the error was of 25 km/h. In this attempt the error is even higher than the one obtained in the first attempt, flight 01.1302. In that case the error at low speeds was about 15 km/h. This result suggests that the presence of the O-ring behind the static port further decreases the stagnation pressure and this brings to the increase of the dynamic pressure value.

**Anemometer calibration – Flight 01.1602**

The last attempt with this type of Pitot tube has been performed with one O-ring behind the static port and one in front of it, this time there was no space between the O-rings and the hole. The configuration is shown in the following figure.

Figure A.0.10: Pitot tube - 5th attempt

As clear from the following figures, there were no substantial changes with this configuration. This umpteenth unacceptable result made sure that the static port position was changed. The new solution will be explained in the following paragraph.

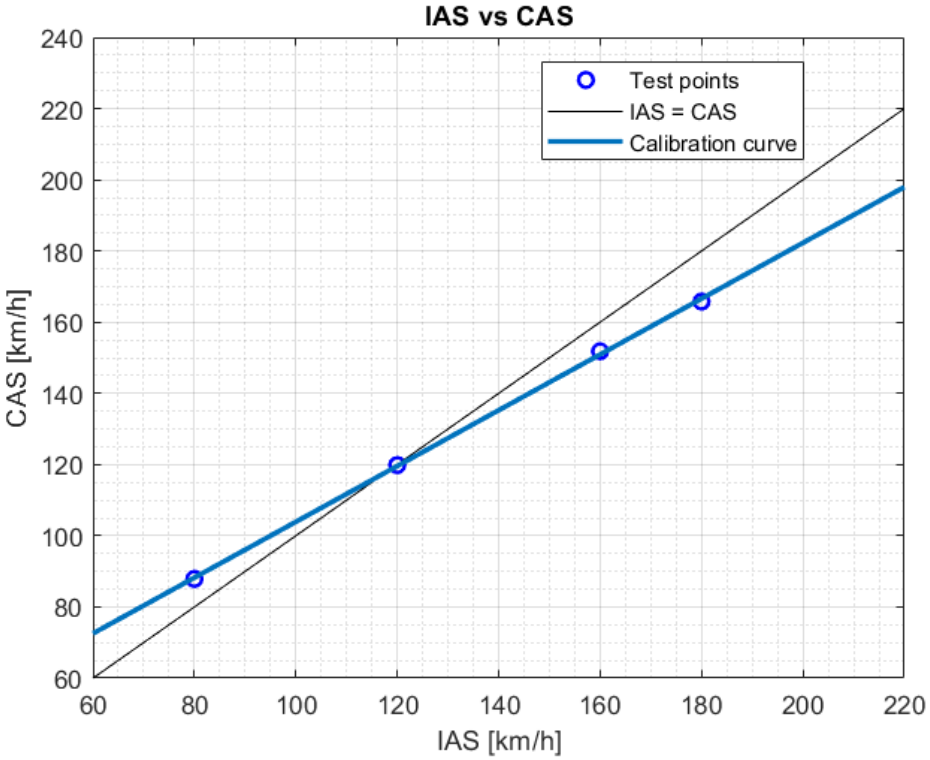


Figure A.0.11: IAS vs CAS - CR configuration - flight 01.1602

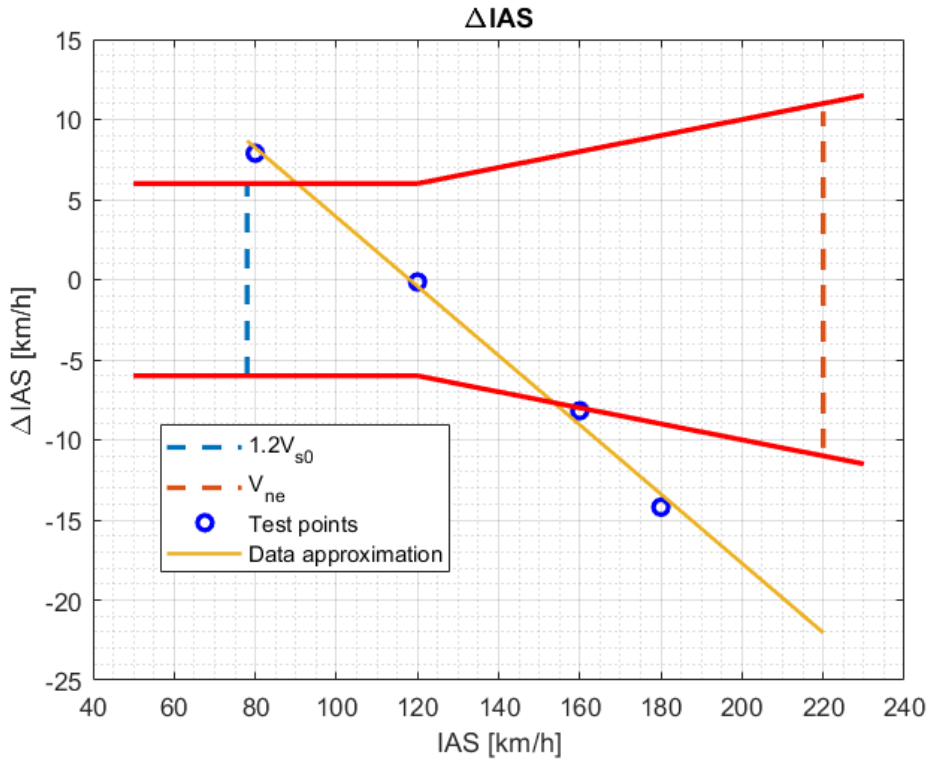


Figure A.0.12: IAS error - CR configuration - flight 01.1602

**Anemometer calibration – Flight 01.3103**

Because of the obtained results, the idea was to change the position of the static port. In particular, in the flight 01.3103, the static pressure tube was detached from the anemometer so it directly read the static pressure present in the cabin. The pitot tube was left under the wing but used only to obtain the total pressure.

As clear from the following figures, also this configuration has to be considered unacceptable. The error is too high just over the 90 km/h.

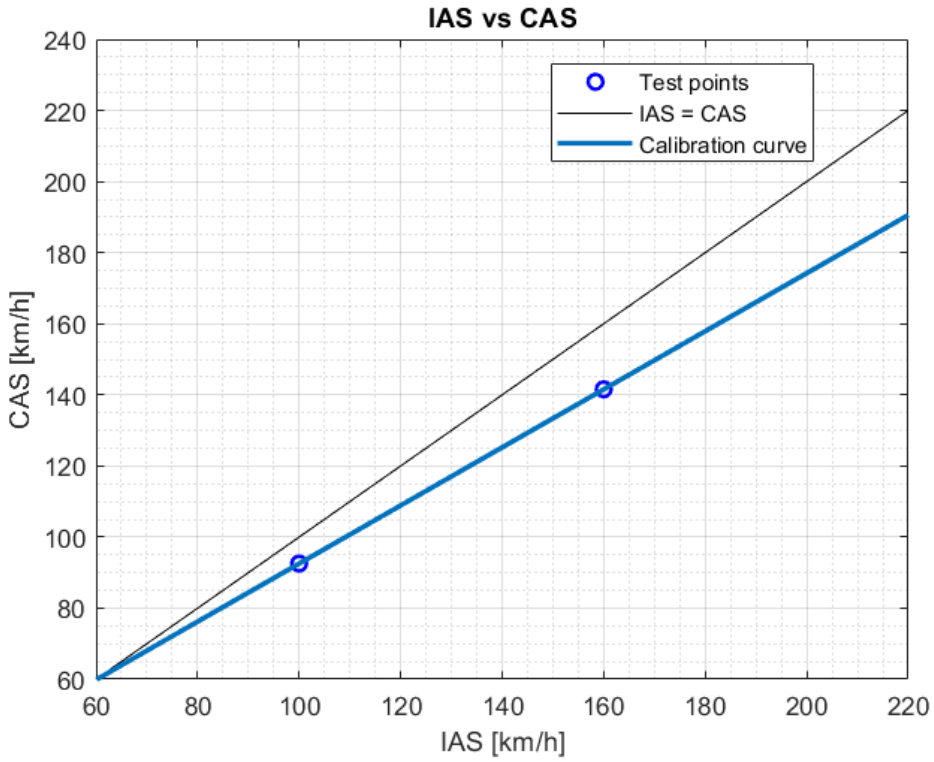


Figure A.0.13: IAS vs CAS - CR configuration - flight 01.3103

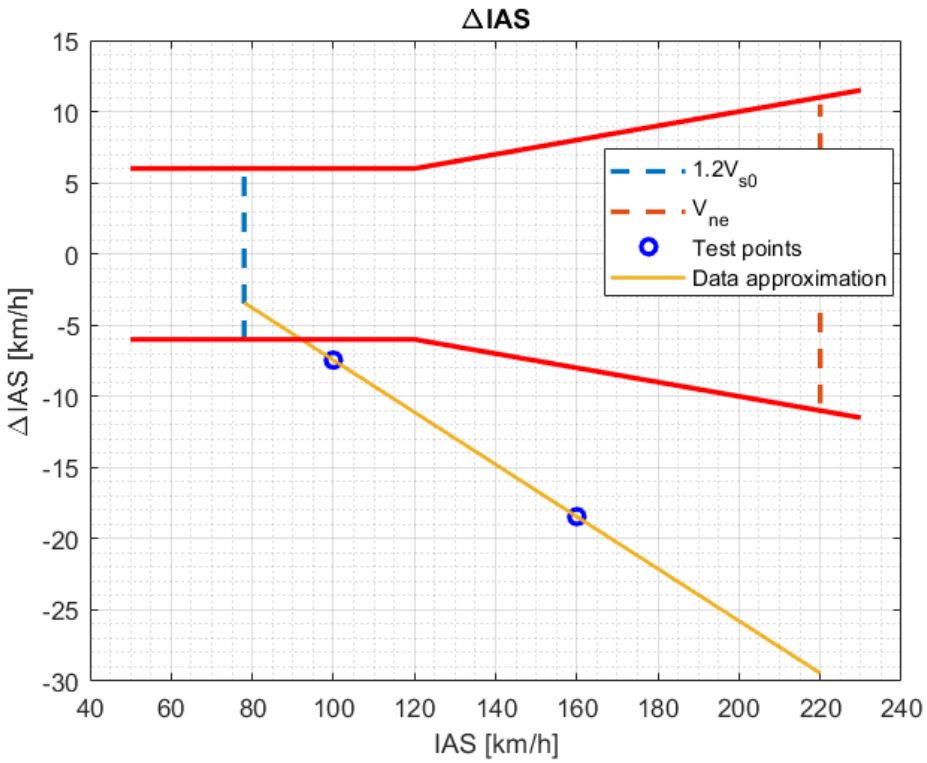


Figure A.0.14: IAS error - CR configuration - flight 01.3103

**Anemometer calibration – Flight 02.3103**

In this 7th attempt the static port was placed on the fuselage, behind the left cockpit door. As clear from *Figure A.0.15*, this was a temporary solution in order to understand if this was the correct way or not.

Figure A.0.15: Static tube - 7th attempt

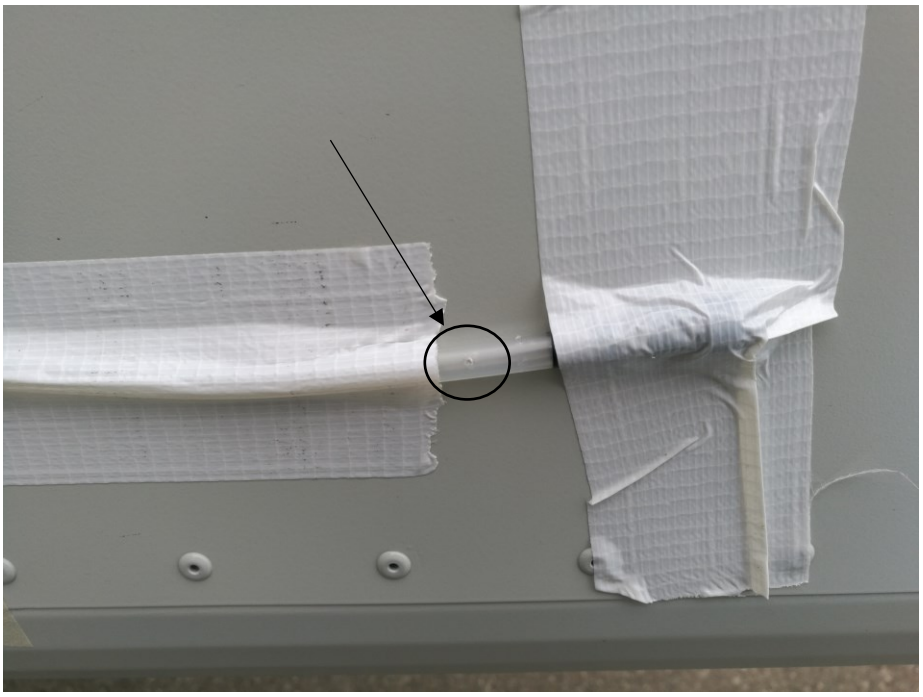

Figure A.0.16: Particular of the small static hole

Finally, this attempt gave the desired results. The results are presented in the following figures.

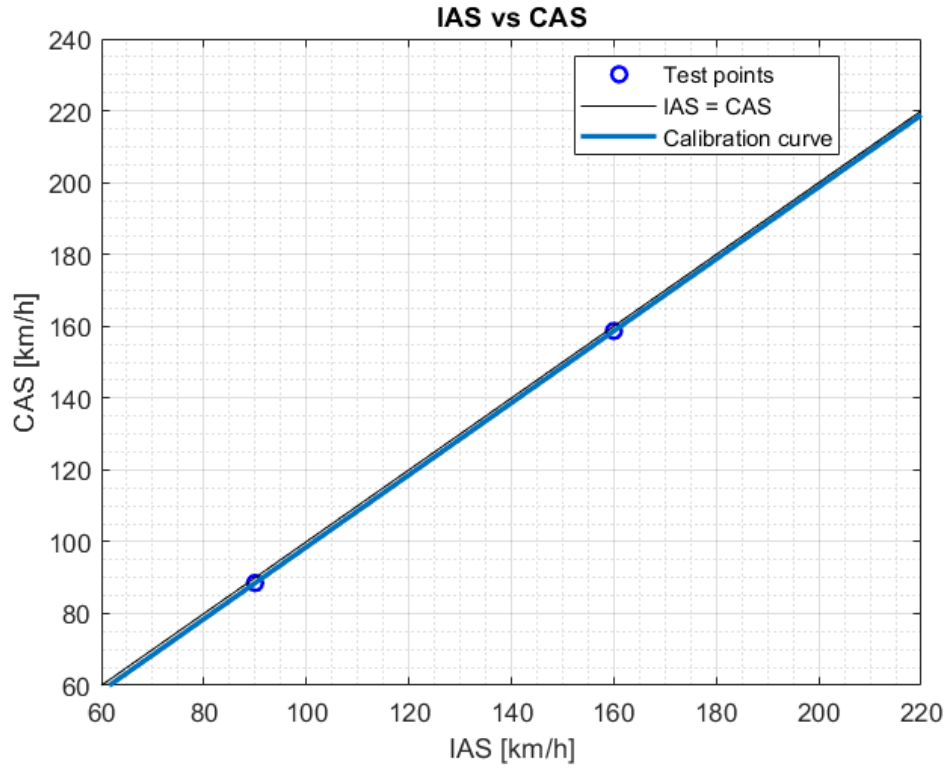


Figure A.0.17: IAS vs CAS - CR configuration - flight 02.3103

From this figure is clear that the calibration line almost coincides with IAS equal to CAS line. This is a very good result, more than the expected. In fact the position error for this configuration results to be 1.5 km/h, as shown in *Figure A.0.18*.

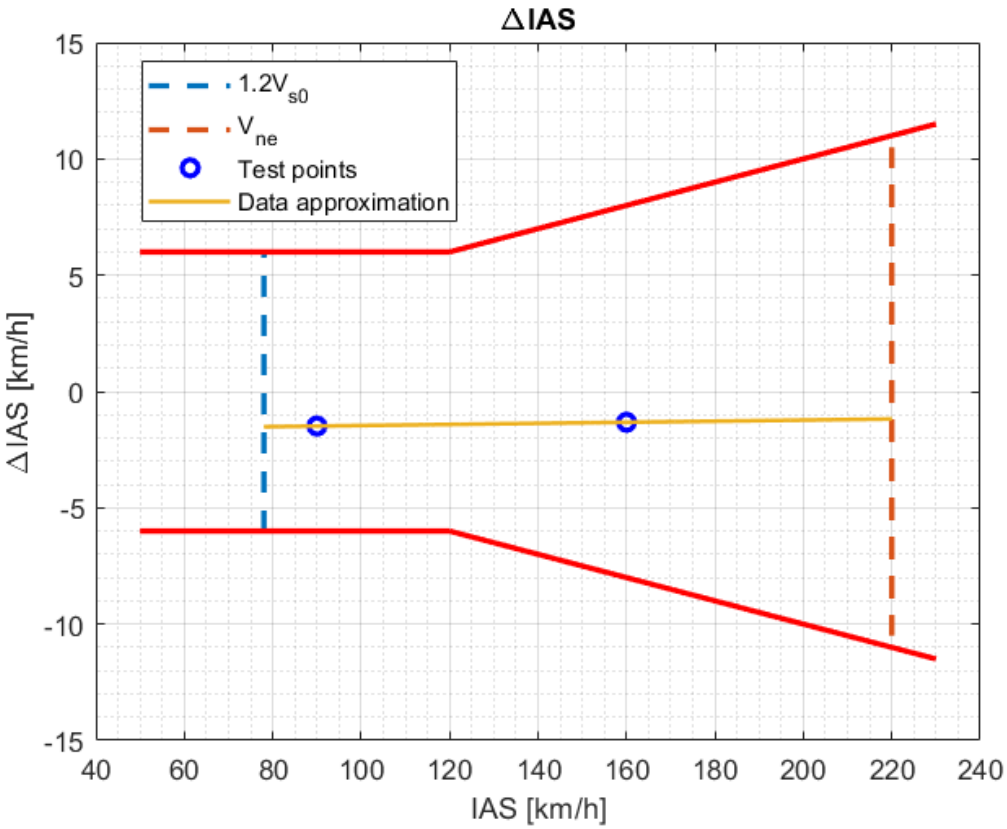


Figure A.0.18: IAS error - CR configuration - flight 02.3103

**Anemometer calibration – Flight 03.3103**

Despite the good results, it was necessary to try a new position of the static probe in order to place it in a better point from an installation point of view.

So the tube was curved in order to have the static port higher than in the previous attempt. The new configuration is here presented.

Figure A.0.19: Static probe - 8th attempt

The error obtained was minor than the one of the flight 02.3103. In this case the error is null. This suggests that this particular point of the fuselage is in a sector where the flow is laminar and thanks to this, the position error is zero.

At this point, a new flight has been performed with a different Pitot tube. In fact, the one mounted in flight 03.3103 had two tubes: one for the total pressure and the other one for the static pressure. It has been substituted with a new one with only one tube used to obtain the total pressure, as explained in the following chapter.

In the following figures, the reader can find proof of what has been said.

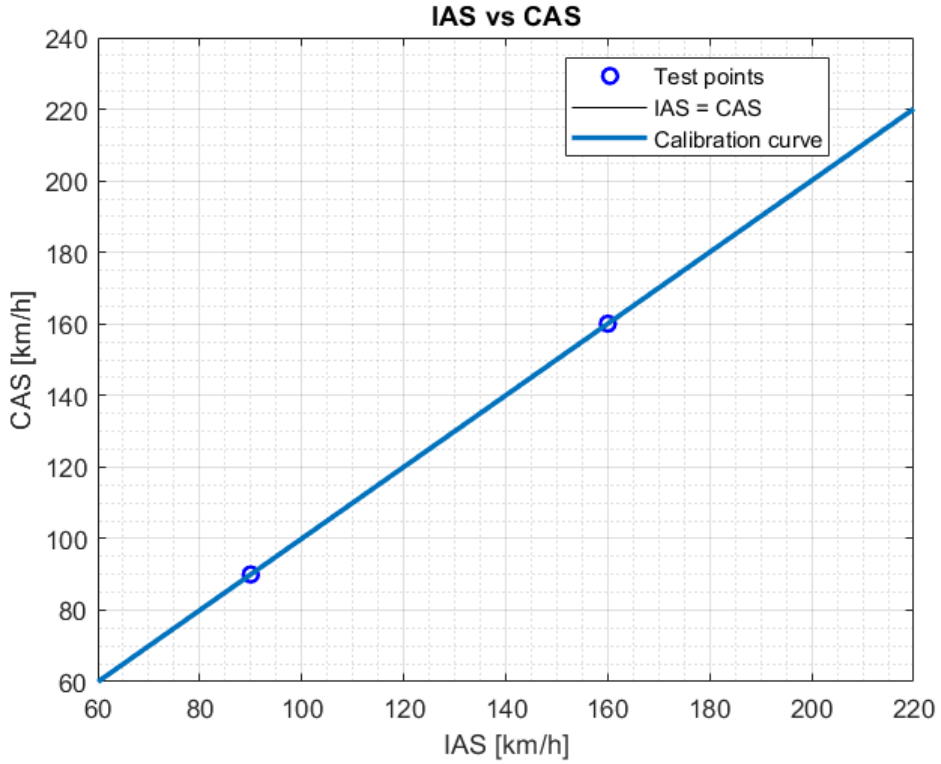


Figure A.0.20: IAS vs CAS - CR configuration - flight 03.3103

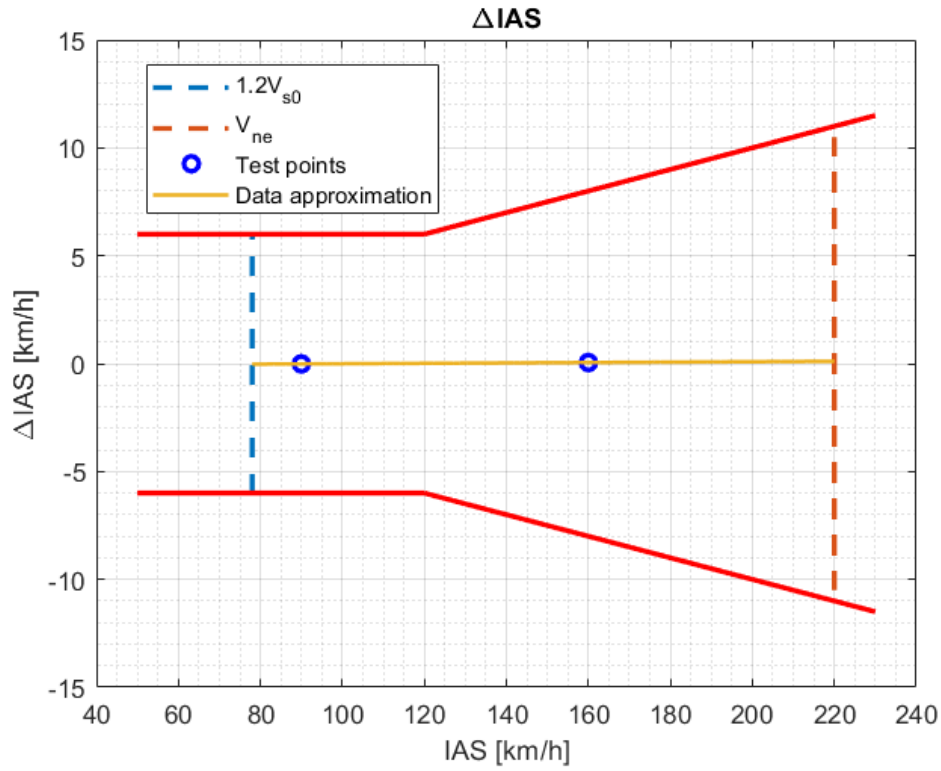


Figure A.0.21: IAS error - CR configuration - flight 03.3103

**Anemometer calibration – Flight 04.3103 and flight 05.3103**

In the fourth flight of the day, the position of the static probe was frozen and the Pitot tube has been substituted with a new one always in the same place, which only has one tube: this has been used to obtain the total pressure. This change has been done in order to standardize the production, in fact this is the total air pressure tube also used on the Ing. Nando Groppo TRAIL.

The test flight has been performed, but the results obtained were unacceptable, as shown in *Figure A.0.23*. In particular, the error results too high at low speeds.

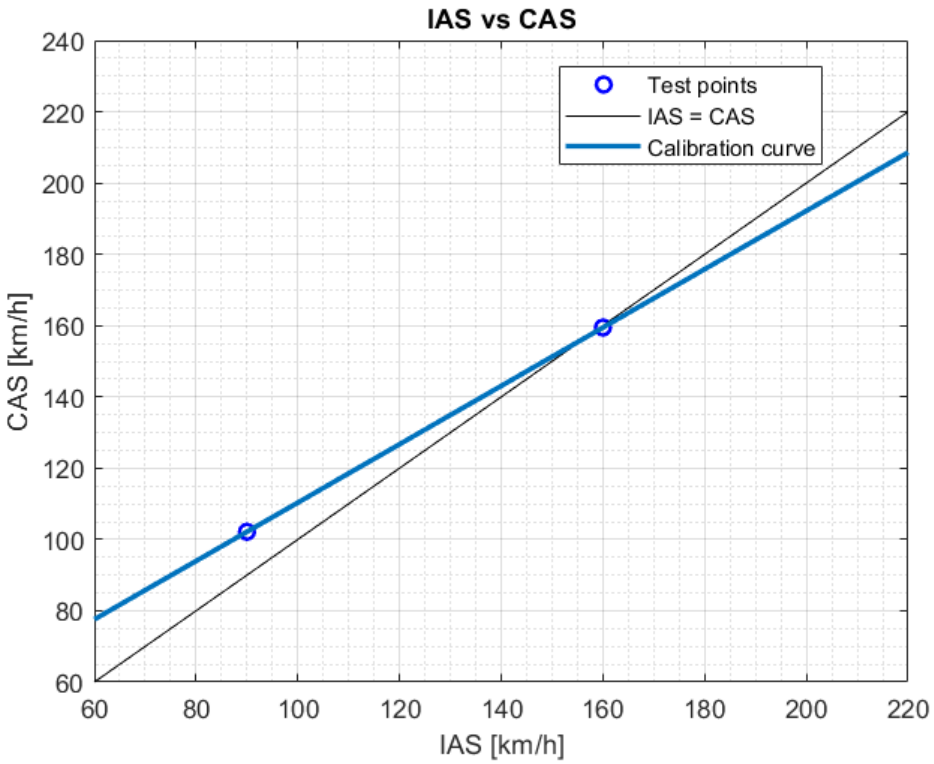


Figure A.0.22: IAS vs CAS - CR configuration - flight 04.3103

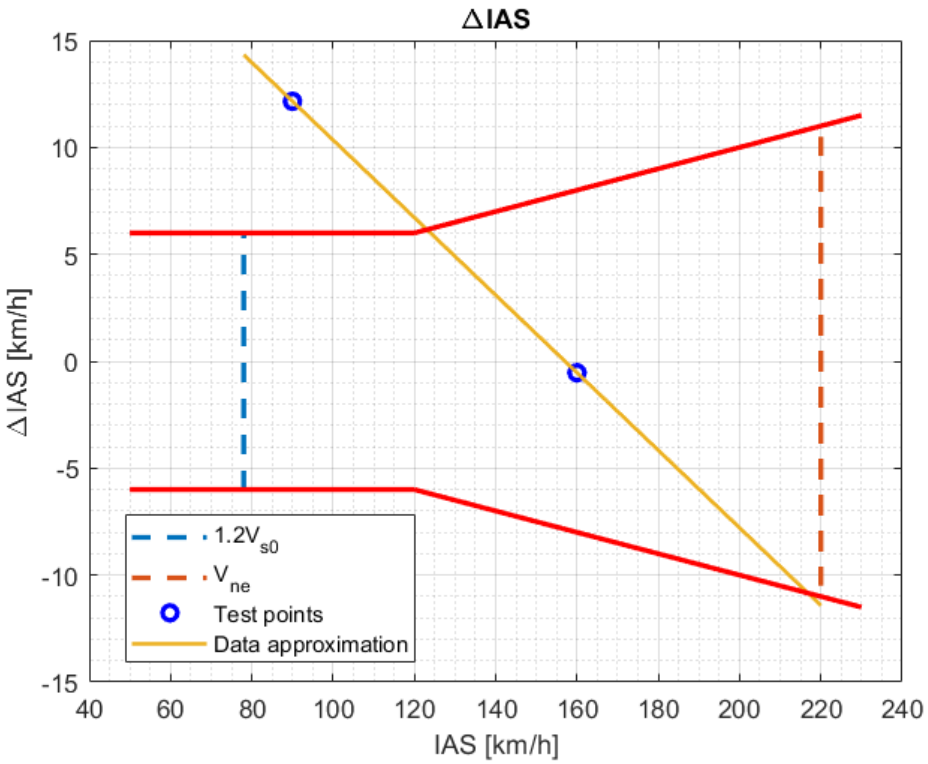


Figure A.0.23: IAS error - CR configuration - flight 04.3103

The reason of this error has been found after an observation of the Pitot tube made by the author. He found that the tube was not aligned with the aircraft but it was inclined 5 degrees. Thanks to this discovery, the new Pitot tube has been mounted with the correct inclination: parallel to the longitudinal axis of the aircraft. *Figure A.0.24* shows the new Pitot tube mounted in the correct way.

Figure A.0.24: G70 new Pitot tube correctly installed

This new configuration gave good results. As clear from the following figures, the IAS error is not null as in flight 03.3103, however it is acceptable with respect to the LTF-UL.

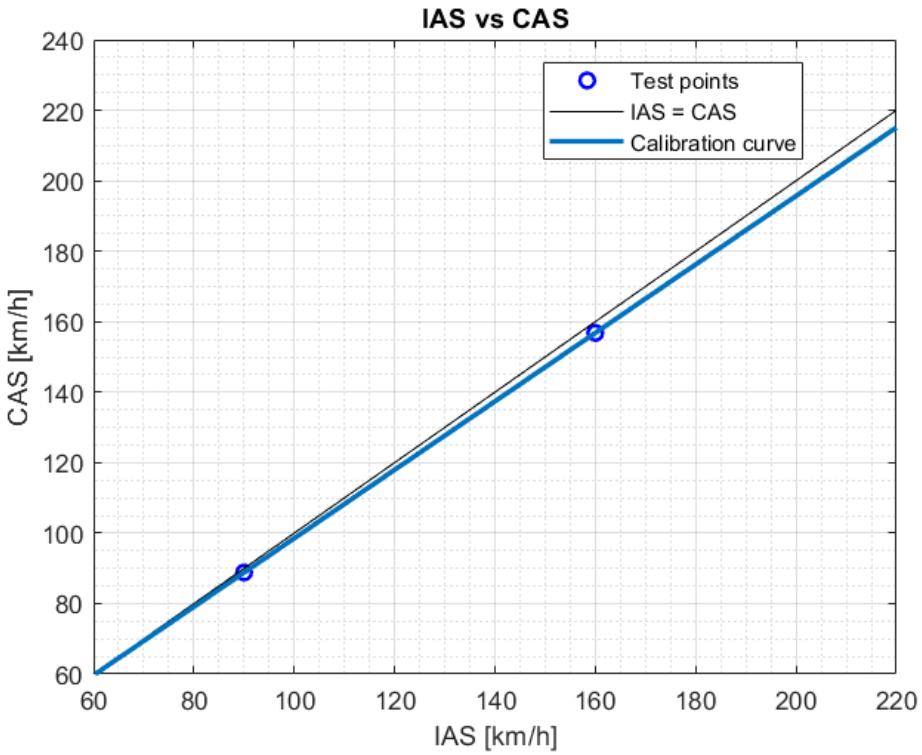


Figure A.0.25: IAS vs CAS - CR configuration - flight 05.3103

In this test flight the error was almost null at low speeds and it slightly increased at higher speeds. At the maximum speed of the A/C the IAS error was about 5 km/h which is the half of the maximum error accepted.

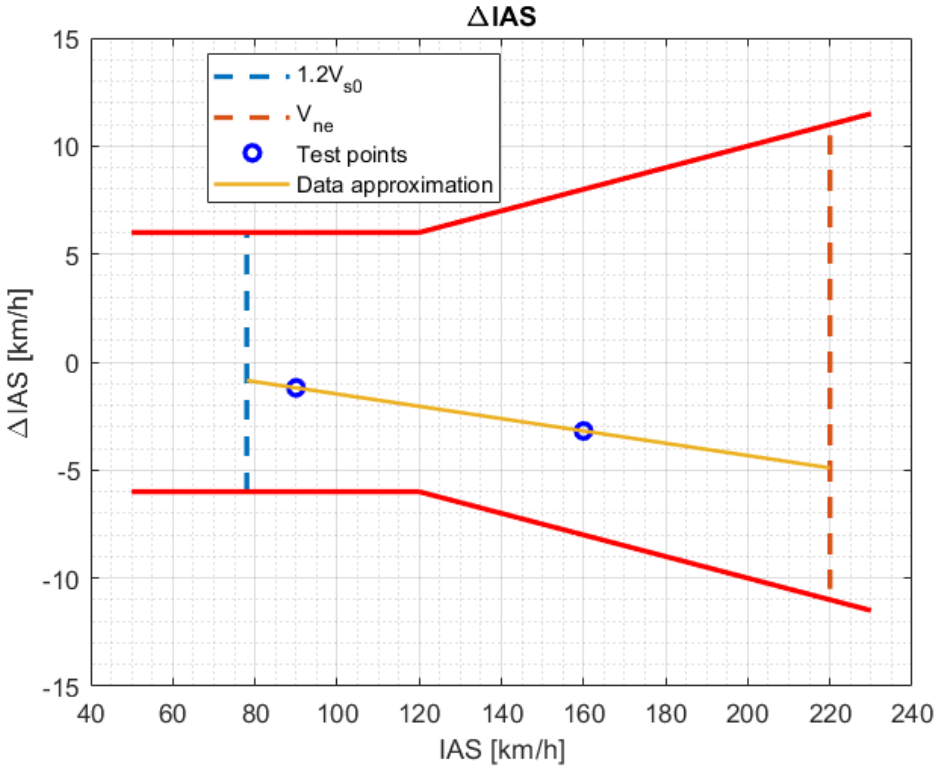


Figure A.0.26: IAS error - CR configuration - flight 05.3103

# Appendix B

# Climb performance theory

During a steady climb, from the horizontal and vertical equilibrium we obtain the following equations:

$$L = W\cos\gamma$$

$$T = D + W\sin\gamma$$

Utilizing the third Newton's law, the previous equation becomes:

$$T - D - W\sin\gamma = Ma = \frac{W}{g}\frac{dV}{dt}$$

We now multiply for TAS and divide for the weight:

$$\frac{V(T-D)}{W} = V\sin\gamma + \frac{V}{g}\frac{dV}{dt}$$

Where $V\sin\gamma$ is the vertical speed. Excess power is defined as

$$Fne = V(T-D)$$

So:

$$Fne = W\frac{dh}{dt} + \frac{W}{g}\frac{dV}{dt}V$$

During a constant TAS climb the second term is null and all the excess energy is utilized to climb. But since during the Sawtooth climb test the climb is performed at constant IAS, the acceleration contribution, which depends on TAS, is not null. This is why one of the corrections explained in the Data reduction chapter includes the TAS gradient with altitude.

# Bibliography

1. Rolando A., Rossi F., Castelletti T., Reghenzani. *Mnemosine Mark-V: The Fifth Generation of an Ultra Light Machine-Dedicated FTI System.* Nuremberg : 27th Annual Society of Flight Test Engineers European Chapter Symposium, 2016.

2. *Legge 25 marzo 1985, n.106 - Disciplina del volo da diporto o sportivo,* Rome, Italy, 1985.

3. *Decreto del Presidente della Repubblica n. 133,* Rome, Italy, 2010.

4. EASA. *Certification Specifications and acceptable means of compliance for Normal, Utility, Aerobatic and Commuter Category Aeroplanes, CS-23 Amendment 4.* 2015.

5. NASA, National Aeronautics and Space Administration. *Information Summaries - Acceleration deceleration.* Houston, Texas, 1995.

6. Ing. Nando Groppo SRL. *Pilot Operating Handbook.* Mezzana Bigli (PV), 03/2018.

7. L., Gardner. *Society of flight test engineers reference handbook.* Lancaster, CA : SFTE, 2001.

8. Lewis, Gregory. *Using GPS to determine Pitot static errors.* National test pilot school professional course series textbooks, Vol. II, Aerodynamics for flight testers, Chapter 7, pitot-statics, Mojave, CA, 2003.

9. http://www.groppo.it

10. Trainelli L., Rolando A., Bonaita G., Chimetto P. *Experiences in academic flight testing education.* Aircraft engineering and aerospace technology, Vol. 86, No. 1, 2014.

11. Rolando A., Trainelli L. *Reliable and Cost-Effective flight testing of ultralight aircraft.* Journal of aircraft, Vol. 48, No. 4, 2011.

12. Trainelli L. Rolando A. Gadarco T. Terzaghi V. Riccobono M. *Flight testing of a new ultralight airplane for LTF-UL certification* . Nuremberg, Germany, 2016.

13. Rolando A. *Development of an integrated flight test instrumentation system for ultra light machines.* Dept. of aerospace engineering, Politecnico di Milano, Milano, Italy, 2008.

14. Stoliker F. *Introduction to flight test engineering.* RTO-AG-300, AC/323 (SCI-FT3)TP/74, Flight test techniques series - Volume 14, North atlantic treaty organisation, Neuilly-sur-Seine, France, 2005.

15. Ward D.T., Strganac T.W. *Introduction to flight test engineering.* Dubuque (IA), USA, Kendall/Hunt, 1998.

16. Kimberlin R.D. *Flight testing of fixed-wing aircraft.* Reston (VA), USA, AIAA education series, 2003.

17. Oldani S. *Comprehensive flight testing and data analysis for a new ultralight aircraft.* Master thesis. Milano, 2017.

18. German civil airworthiness requirements, LTF-UL 2003. *Airworthiness requirements for three axes standard control ultra light aircraft.* Germany, 2003.